

Article

Shear Strength Prediction Equations and Experimental Study of High Strength Steel Fiber-Reinforced Concrete Beams with Different Shear Span-to-Depth Ratios

Wisena Perceka ¹, Wen-Cheng Liao ^{2,*} and Yung-Fu Wu ²

¹ Department of Civil Engineering, Faculty of Engineering, Parahyangan Catholic University, No. 94, Ciumbuleuit Road, Bandung 40141, Indonesia; wperceka@unpar.ac.id

² Department of Civil Engineering, College of Engineering, National Taiwan University, No. 1, Sec. 4, Roosevelt Road, Taipei 10617, Taiwan; r01521239@ntu.edu.tw

* Correspondence: wcliao@ntu.edu.tw

Received: 16 October 2019; Accepted: 5 November 2019; Published: 9 November 2019



Abstract: Conducting research on steel fiber-reinforced concrete (SFRC) beams without stirrups, particularly the SFRC beams with high-strength concrete (HSC) and high-strength steel (HSS) reinforcing bars is essential due to the limitation of test results of high strength SFRC beams with high strength steel reinforcing bars. Eight shear strength prediction equations for analysis and design of the SFRC beam derived by different researchers are summarized. A database was constructed from 236 beams. Accordingly, the previous shear strength equations can be evaluated. Ten high-strength SFRC beams subjected to monotonic loading were prepared to verify the existing shear strength prediction equations. The equations for predicting shear strength of the SFRC beam are proposed on the basis of observations from the test results and evaluation results of the previous shear strength equations. The proposed shear strength equation possesses a reasonable result. For alternative analysis and design of the SFRC beams, ACI 318-19 shear strength equation is modified to consider steel fiber parameters.

Keywords: steel fiber reinforced concrete beam; shear strength; high strength concrete; fiber effectiveness factor; flexural-shear failure; shear failure

1. Introduction

Using high-strength concrete (HSC) with compressive strength exceeding 70 MPa and high-strength steel (HSS) with yield stress of 685 MPa or greater can reduce the member section size and the volume of concrete and steel bars for the entire building structure [1]. The durability of concrete can be improved, owing to lower water-to-cementitious materials ratio of the HSC as well [2]. However, concrete becomes more brittle as its compressive strength increases and greater transverse reinforcement is required accordingly [2–5]. Short and discontinuous steel fiber can be used as an alternative material to improve the ductile behavior of concrete [2,6–9]. Previous research studies have shown that adding steel fibers to concrete beams could enhance shear resistance, toughness, promote flexural failure and ductility, and potentially act as a substitute for conventional shear reinforcement [10–17]. In addition, the randomly oriented steel fibers provide bridging action across the microcracks in the matrix and improve resistance to crack opening [2,9,18–20]. The shear stress on the interface between the steel fibers and the surrounding matrix (bond strength between steel fibers and matrix) is a key parameter in the bridging role and in providing more tensile strength during fracturing. Concrete fails once the steel fibers either break or are completely pulled out from the concrete.

Despite the advantages of steel fibers as reinforcement in the concrete beams, the number of research studies on high-strength steel fiber-reinforced concrete (SFRC) beam with HSS longitudinal bar is limited. The general behavior of SFRC beams is presented in a literature review in order to fully describe the parameters affecting ultimate shear strength of the SFRC beams. In this study, the current shear strength equations for design and analysis of the SFRC beams derived from different research studies are summarized. A database is constructed from 236 beams that consist of normal reinforced concrete and SFRC beams. Every shear strength in the database is compared with the existing shear strength prediction equations. Furthermore, the high-strength SFRC beam specimens were provided to be subjected to monotonic loading. Accordingly, the current shear strength prediction equations can be verified. The new equation for predicting shear strength is proposed based on the evaluation of shear strength equations studied in this paper.

2. Literature Review

2.1. The General Behavior of SFRC Beams

As summarized by Dinh in 2009 [21], the steel fibers perform a role similar to that of shear reinforcement in the transversally-reinforced concrete beam. The presence of steel fibers supports the redistribution of tensile stress, prevents the propagation and opening of diagonal cracks, and is effective for controlling cracks and fostering the formation of multiple diagonal cracks. Furthermore, like shear reinforcement, the steel fibers can delay early concrete splitting along the tensile reinforcing bar. It is known that the orientation and distribution of steel fibers in concrete may not be well controlled due to possible segregation and fiber balling issues; therefore, the shear strength analysis for an SFRC beam faces several challenges. The proper distribution of the steel fibers for the improvement of mechanical properties is also the most important issue related to the steel fiber reinforcement in an SFRC member. Unlike normal concrete, the opening of wide diagonal cracks in an SFRC beam is the result of fiber pullout rather than shear reinforcement yielding. Moreover, the pullout behavior of steel fibers and the bond strength between the steel fibers and the concrete remain a complex problem [21]. The shear behavior of a simply-supported SFRC beam subject to two-point concentrated and monotonic loads is affected by beam cross section (shape and size), ratio of shear span-to-effective depth, tensile reinforcement ratio, concrete compressive strength, size of coarse aggregate, fiber volume fraction, and the bond stress between steel fibers and the surrounding matrix. The commonly considered parameters for calculating SFRC ultimate shear stress are the shear span-to-effective depth, the longitudinal tensile reinforcement ratio, the concrete compressive strength, the fiber volume fraction, and the bond stress between steel fibers and the surrounding matrix.

The shear span-to-effective depth ratio has a significant effect on the SFRC ultimate shear strength, as shown in previous research studies. The arch action occurring in a beam with smaller shear span transfers load from the loading point to the support directly through a compressive strut. Dinh [21] reported that Batson et al. in 1972 proposed a critical value of a shear span-to-effective depth ratio of 3 for the SFRC beams. The relationship between normalized shear strength and the shear span-to-effective depth ratio reported by different researchers is shown in Figure 1 [11]. The symbols V_u , b_w , d , f'_c , a , ρ , f_{yl} , $f_{u,SF}$, and V_f shown in Figure 1 stand for beam ultimate shear strength, beam section width, section effective depth, concrete compressive strength, shear-span length, longitudinal reinforcement ratio, yield strength of longitudinal reinforcing bar, ultimate tensile strength of steel fiber, and fiber volume fraction, respectively. It can be seen that the beam shear strength becomes smaller, as the shear span-to-effective depth ratio increases.

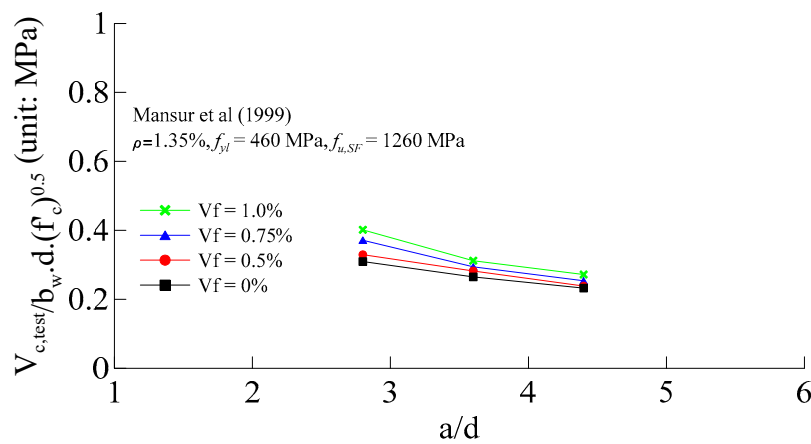


Figure 1. The relationship between normalized shear stress and shear span-to-effective depth ratio [11].

The longitudinal tensile reinforcement ratio in an SFRC beam was investigated as well. The SFRC beam with greater longitudinal tensile reinforcement ratio can resist more ultimate shear strength due to an increase of dowel action and height of compression zone [13,22]. In general, the steel fibers must contribute to improving the dowel strength, since steel fibers provide bridging action across the microcracks in the matrix and improve resistance to crack opening. Swamy and Bahia [23] conducted an experimental study, in which they provided several beam specimens. They reported that the concrete strain prior to dowel cracking varied between 600×10^{-6} to 850×10^{-6} , where these values were relatively high compared to the maximum tensile strain of normal and even fiber reinforced concrete. As reported by Zarrionpour and Chao [24], the dowel action in the slender SFRC beams varied between 10 to 35% of the total shear capacity as the height of beam varied between 305 to 1220 mm, and the shear span-to-effective depth ratio of tested beams ranged from 3.45 to 3.6. Therefore, according to research conducted by Swamy and Bahia [23] and Zarrionpour and Chao [24], the dowel action contributed to the shear strength of SFRC beams. On the other hand, Dinh et al. [25] reported that the shear contribution of dowel action was ignored according to the test results of 24 beams (4 plain concrete beams and 20 SFRC beams). The failure mode for plain concrete beams was diagonal tension, while 18 SFRC beams failed due to shear tension. Figure 2 shows the relationship between the normalized shear strength and the longitudinal tensile reinforcement ratio for different shear-span-to-effective depth ratios. It can be seen that the longitudinal tensile reinforcement ratio improves the SFRC shear strength, regardless of the contribution of dowel action.

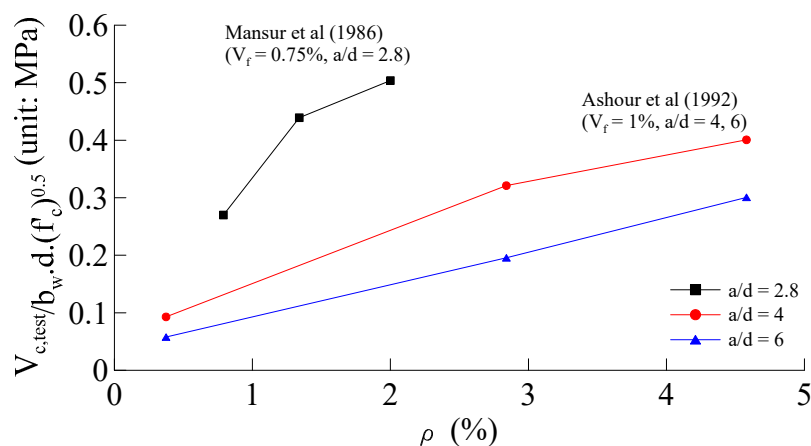


Figure 2. Relationships between normalized shear stress and longitudinal tensile reinforcement ratio [11,13].

The concrete compressive stress is one of the important parameters for ultimate shear strength of the SFRC beam. It can be observed from research conducted by Kwak et al. [17] that when the concrete compressive strengths were increased up to 100%, while other parameters remained the same, the improvements of ultimate shear strength were 26%, 21%, and 20% for beams with shear span-to-effective depth ratio of 2, 3, and 4, respectively.

In regard to the contribution of aggregate size to shear capacity, greater aggregate size in the SFRC beam could enhance the shear resistance of the beam due to increased aggregate interlock [21]. To be on the safe side, most researchers selected aggregate with maximum size of 9.5 mm accordingly [21]. Zarrionpour and Chao [24] measured the shear resistance from aggregate interlock at any point along crack length with a crack width exceeding 0.2 mm. It was reported that the contribution of aggregate interlock to shear resistance ranged from 0 to 5% [24]. Also, it was reported that the aggregate interlock in the SFRC beams had a minor contribution at the point where the beams reached their peak strength.

The last two important parameters are the fiber volume fraction and the bond strength of the fiber-matrix interface. The effect of fiber volume fraction on shear strength also depends on fiber diameter and fiber length [21]. The table in Appendix A presents the shear stresses of SFRC beams with different fiber volume fraction and aspect ratio, where those results are part of the experimental results collected in this study. It can be seen that when the fiber volume fraction and the steel fiber aspect ratio are varied, while other parameters remain the same, there is almost no difference in the shear stresses. For example, it can be found from the test results conducted by Dinh et al. [25], in which 4 SFRC beams contained 2 different steel fiber aspect ratios and fiber volume fractions, while other parameters remained the same. The specimens B18-3c, B18-3d, B18-5a, and B18-5b had similar ultimate shear stress. This is because specimens B18-3c, B18-3d, B18-5a, and B18-5b had a similar reinforcing index for steel fiber, RI, in which RI is a multiplication of the steel fiber aspect ratio and the fiber volume fraction. Improving the fiber volume fraction may improve shear strength significantly, if the fiber volume fraction is the only parameter improved, while other parameters, including steel fiber aspect ratio, are kept to remain the same [11,26].

The bond strength of the fiber-matrix interface has usually been neglected. Swamy et al. [27] set the bond strength between steel fibers and concrete matrix at 4.15 MPa. Liao et al. [2] and Perceka et al. [9] conducted single-fiber pullout tests to determine the equivalent bond strength that describes the bond strength of the fiber-matrix interface. In order to account for the equivalent bond strength, τ_{eq} , Equation (1) that was proposed by Kim et al. [2] can be used. In addition, Liao et al. [2] and Perceka et al. [9] used micromechanical model proposed by Xu et al. in 2011 [2,9] to verify the experimental results. Both authors reported that the difference between the experimental and analytical results was only 10% [2].

$$\tau_{eq} = 2E_{pullout}/\pi D_f L_e^2 \quad (1)$$

where $E_{pullout}$ is the pullout energy defined as an area under a pullout force-slip curve, D_f is fiber diameter, and L_e is the length of fiber embedded in the matrix.

2.2. Shear Strength Prediction Equations

The number of equations used to predict the shear strength of SFRC beams without shear reinforcement can be found in many research studies. Selected shear strength prediction equations for the SFRC beam without shear reinforcement proposed by previous researchers are shown in Equations (2)–(12).

Sharma [10]:

$$V_{c,SF} = \frac{2}{3} f'_t (d/a)^{0.25} b_w d \quad (2)$$

where f'_t is the concrete tensile strength based on split-cylinder test.

Narayan and Darwish [12]:

$$V_{c,SF} = \left(e \left[0.24 f_{spfc} + 80 \rho^d/a \right] + v_b \right) b_w d \quad (3)$$

$$\text{With } f_{spfc} = f_{cu}/(20 - \sqrt{F}) + 0.7 + 1.0 \sqrt{F}; F = (L_f/D_f)V_f d_f \text{ and } v_b = 0.41\tau F \quad (4)$$

where f_{spfc} is the computed value of split-cylinder strength of fiber concrete, F is the fiber factor; f_{cu} is the cube strength of fiber concrete, L_f is the steel fiber length, τ is the average fiber interfacial bond stress that can be taken as 4.15 MPa [17], d_f is the bond factor: 0.5 for round fibers, 0.75 for crimped fibers, and 1.00 for indented fibers, v_b the shear stress provided by steel fibers, e is the arch action that is equal to 1.0 for $\frac{a}{d}$ greater than 2.80 and equal to $2.8\frac{d}{a}$ for $\frac{a}{d}$ less than 2.80.

Ashour et al. [13]:

The first equation (Equations (5a) and (5b)):

$$\text{for } a/d \geq 2.5, V_{c,SF} = \left(2.11 \sqrt[3]{f'_c} + 7F\right)(\rho d/a)^{0.333} b_w d \quad (5a)$$

$$\text{for } a/d < 2.5, V_{c,SF} = \left[\left(2.11 \sqrt[3]{f'_c} + 7F\right)(\rho d/a)^{0.333} \frac{2.5}{(a/d)} + v_b(2.5 - a/d)\right] b_w d \quad (5b)$$

The second equation (Equation (6)):

$$V_{c,SF} = \left[\left(0.7 \sqrt{f'_c} + 7F\right)d/a + 17.2\rho d/a\right] b_w d \quad (6)$$

Parra-Montesinos [15]:

Parra-Montesinos in 2006 summarized the test data from beams subjected to shear force and reported the use of deformed steel fibers as an alternative minimum stirrups for beams subjected to factored shear forces ranging from $0.085 \sqrt{f'_c} b_w d$ to $1.7 \sqrt{f'_c} b_w d$ (in SI units). The range of those values corresponds to $0.5V_c$ and V_c . The SFRC beams with a fiber volume fraction of 0.75% or greater exhibited ultimate shear stresses that were greater than the conservative lower bound value of $0.3 \sqrt{f'_c}$ MPa. Therefore, the shear strength of SFRC beam can be expressed in Equation (7).

$$V_{c,SF} = 0.3 \sqrt{f'_c} b_w d \text{ (N)} \quad (7)$$

Kwak et al. [17]:

Kwak et al. in 2002 conducted an experimental program and proposed equations to predict the shear strength of SFRC beams, as shown in Equation (8). The shear strength prediction equation is expressed in Equation (8a).

$$V_{c,SF} = \left(3.7 e f_{spfc}^{\frac{2}{3}} (\rho d/a)^{1/3} + 0.8v_b\right) b_w d \quad (8a)$$

where e is shown in Equation (8b).

$$e = 1.0 \text{ for } a/d > 3.4, \text{ and } 3.4 d/a \text{ for } a/d \leq 3.4 \quad (8b)$$

Dinh [21]:

The proposed shear strength is expressed in Equation (9), where the first and second terms are the contribution of the beam compression zone to shear strength and shear strength provided by steel fibers, respectively. It shall be noted that $0.11f'_c$ is the uniform shear stress that is associated with the normal stress of $0.85f'_c$. This shear stress is assumed to act over the depth of the compression zone. Furthermore, the contribution of steel fibers to shear strength was derived by assuming the transferred tensile force across the critical crack through fiber tension depending on the crack width. The magnitude of that tensile force was estimated by using the constant stress rather than actual

distribution. In order to simplify the derivation process, the tensile force below the tensile longitudinal reinforcing bar was ignored.

$$V_{c,SF} = \left(\frac{0.11f'_c \beta_1 c + (\sigma_t)_{avg} (d - c) \cot(\alpha)}{d} \right) b_w d \quad (9)$$

$$\text{with : } (\sigma_t)_{avg} = 0.8 \times 1.5 \left(\frac{V_f}{0.0075} \right)^{\frac{1}{4}} \quad (10)$$

where c is the depth of neutral axis; β_1 is the ratio of equivalent rectangular compressive stress block depth-to-neutral axis depth; α is the angle for critical inclined crack (set as 45 degree); and $(\sigma_t)_{avg}$ is the average tensile stress.

Wu [28]:

Wu modified Dinh's shear strength model (2014). The uniform shear stress is $0.12f'_c$ instead of $0.11f'_c$. This uniform shear stress corresponded with the normal stress of $0.80f'_c$. In addition, the strain in the extreme layer of the concrete compression zone was assumed to be 0.004 rather than 0.003 from the regression results of SFRC cylinder tests. The shear strength model proposed by Wu is given in Equation (11), in which the parameters λ_1 , λ_2 , and λ_3 are defined as 0.25, 1.2, and 1, respectively.

$$V_{c,SF} = \left(\frac{0.12f'_c \beta_1 c + \sigma_{pc} (h - c) \cot(\alpha)}{d} \right) b_w d \quad (11)$$

$$\text{with } \sigma_{pc} = \lambda_1 \lambda_2 \lambda_3 \frac{L_f}{D_f} V_f \tau_{eq} \quad (12)$$

where h is the beam section height; σ_{pc} is the post-cracking stress; and $\lambda_1 \lambda_2 \lambda_3$ is the factor relating fibers pullout ratio, efficiency factor of orientation in the crack state, and the number of fibers pulling out per unit area.

2.3. Evaluation of Shear Strength Prediction Equations

Eight equations are compared with test results. Two-hundred thirty-six test results from reinforced concrete and SFRC beams without shear reinforcement and with concrete compressive stress ranging from 20.6 to 194 MPa, shear span-to-effective depth ratio ranging from 1.0 to 6.0, and fiber volume fraction ranging from 0 to 2%, are collected [11,13,17,21,24–26,29–39]. The relationship between measured and predicted shear strengths using previous shear strength prediction equations is shown in Figure 3. The statistic evaluation results, namely mean and coefficient of variation (COV) values for comparison between measured and predicted strengths are summarized in Table 1 and shown in Figure 3 as well. If a data point appears above the solid line, the measured strength is greater than the predicted stress; otherwise, the predicted strength is greater than the measured strength. Two dashed lines are shown as boundaries with 20% offset from the predicted shear strength.

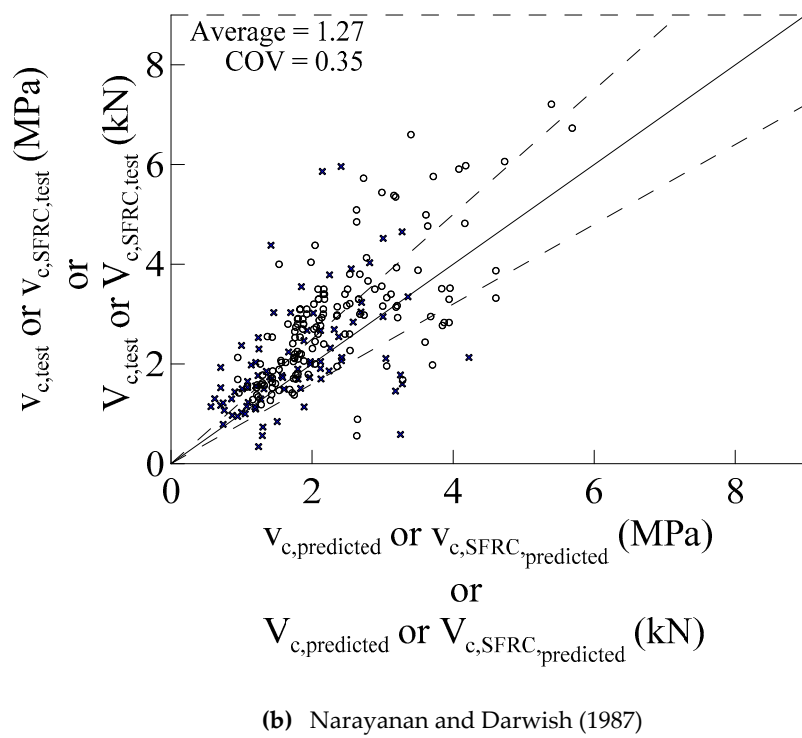
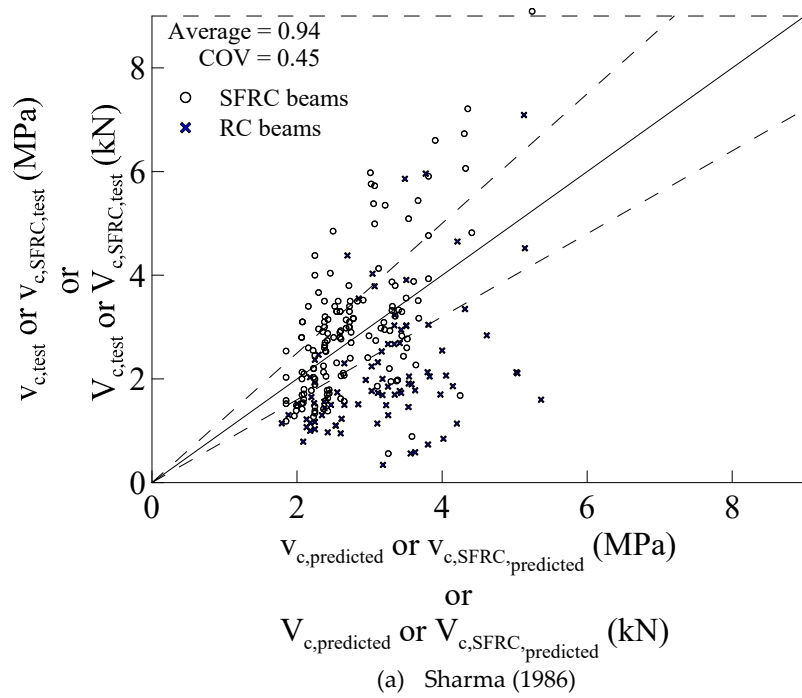
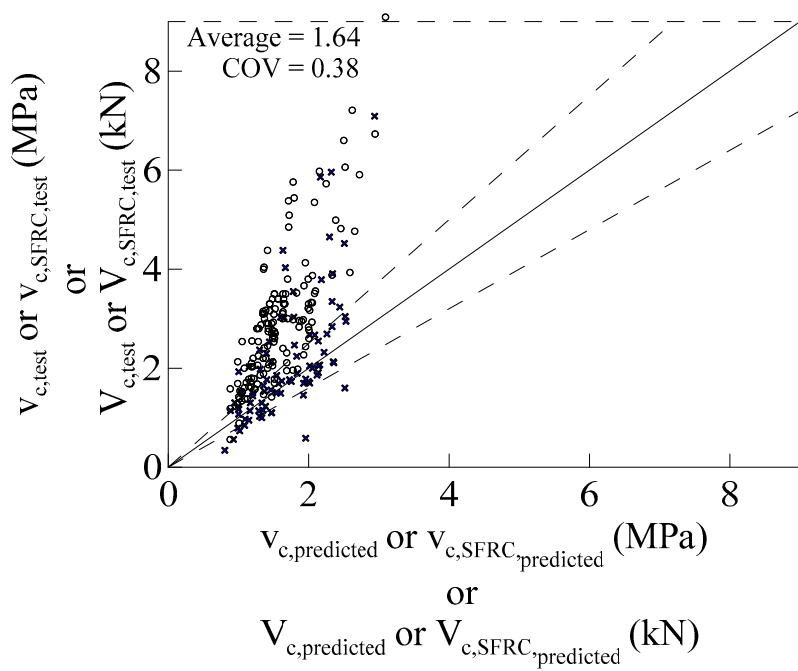
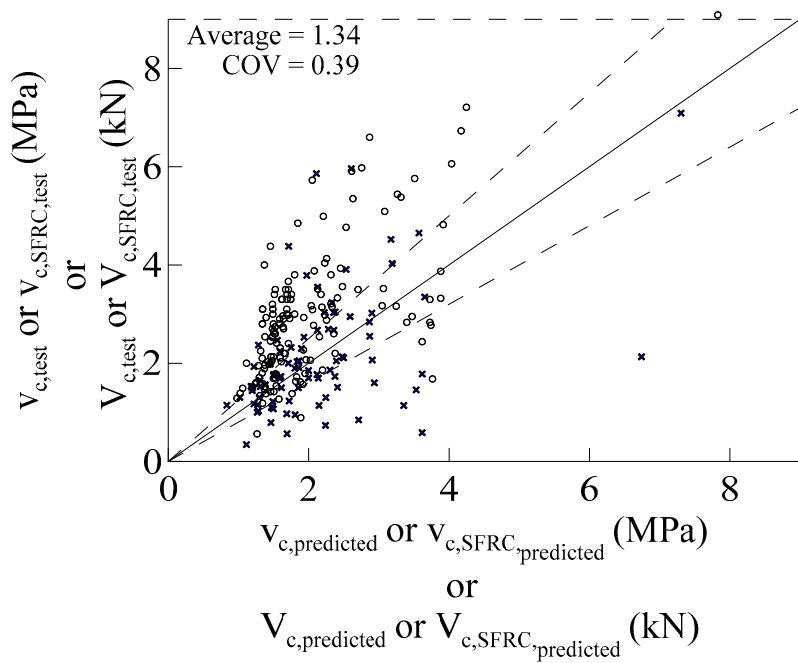


Figure 3. Cont.

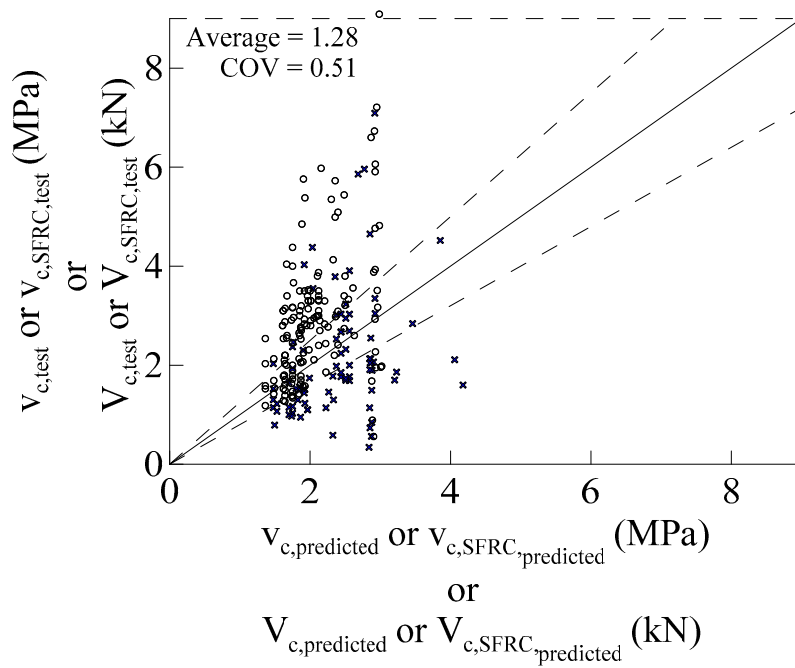


(c) Ashour et al. (1992) [Equation (5a)]

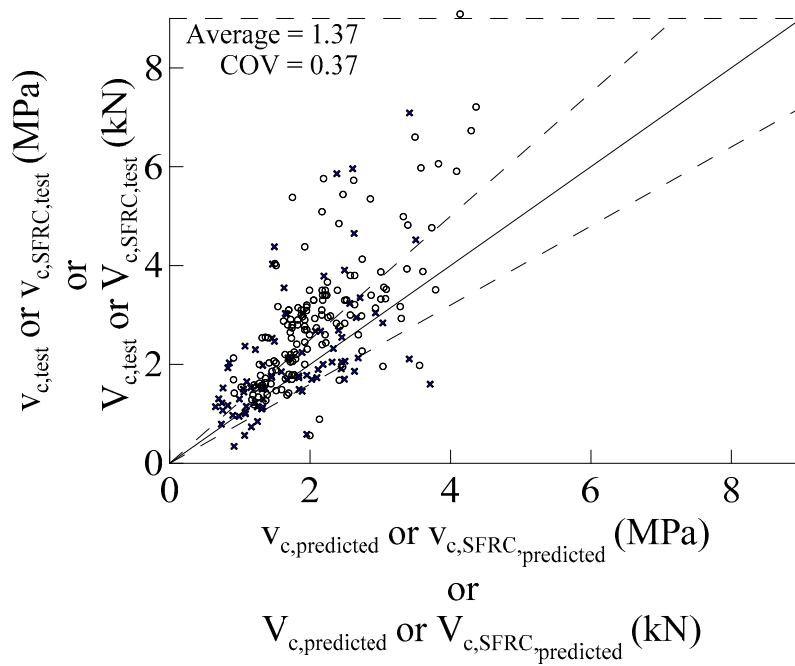


(d) Ashour et al. (1992) [Equation (6)]

Figure 3. Cont.

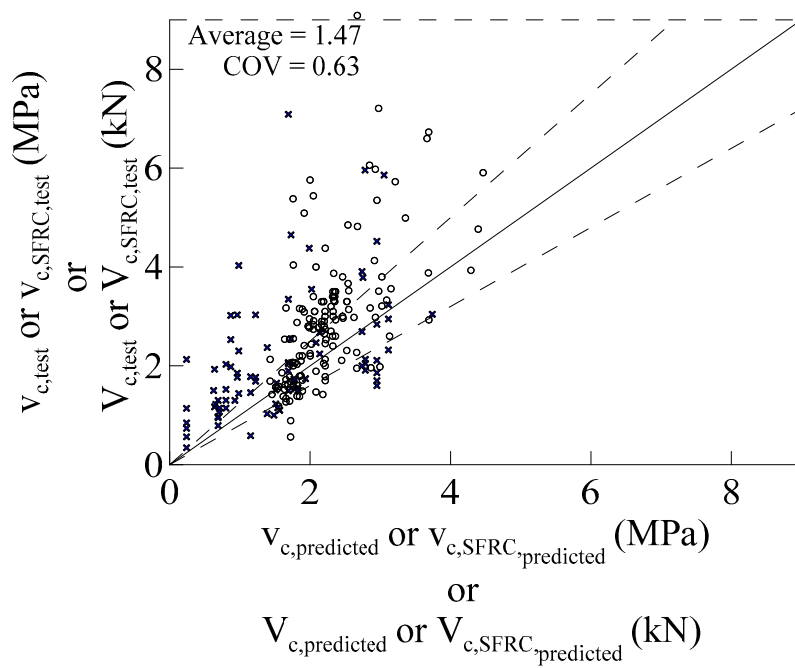


(e) Parra-Montesinos (2006)

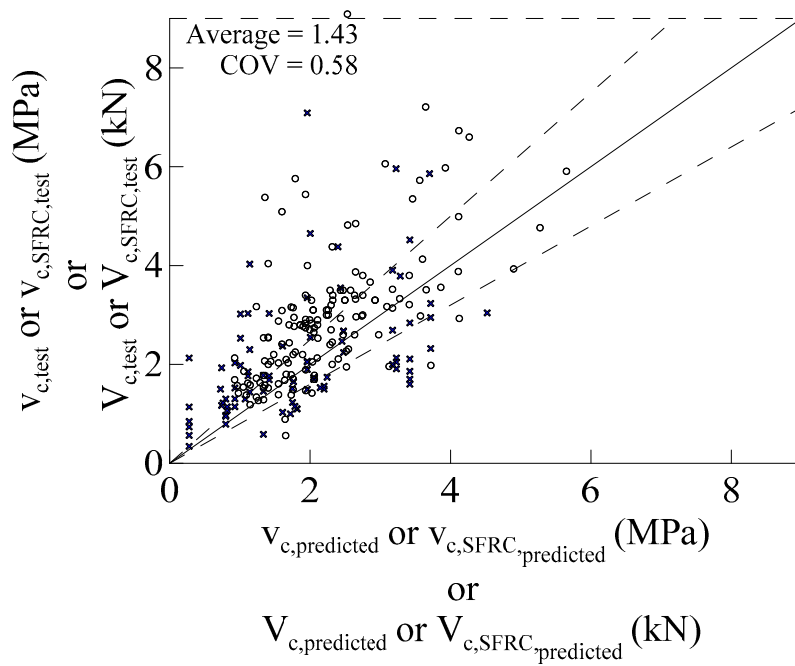


(f) Kwak et al. (2002)

Figure 3. Cont.



(g) Dinh (2011)



(h) Wu (2014)

Figure 3. Comparison between measured and predicted shear strengths.

Table 1. Statistical evaluation results for comparison between measured and predicted shear strengths.

Shear Strength Model		Mean of $V_{c,exp}/V_{c,pre}$	COV
Sharma (1986)		0.94	0.45
Narayanan and Darwish (1987)		1.27	0.35
Ashour et al. (1992)	Equation (5a)	1.64	0.38
	Equation (6)	1.34	0.39
Parra-Montesinos (2006)		1.28	0.51
Kwak et al. (2002)		1.37	0.37
Dinh (2011)		1.47	0.63
Yung-Fu Wu (2014)		1.43	0.58

The shear strength model proposed by Sharma (Equation (2)) tends to overestimate the shear strength of SFRC beam. One-hundred specimens appear below the lower dashed line, which means that the measured shear strength values of 100 specimens are less than 80% of the corresponding predicted shear strength values. On the other hand, the measured shear strength values of 57 specimens are greater than 120% of the corresponding predicted shear strength values. Calculated shear strength values using the model proposed Narayanan and Darwish (Equation (3)) and Ashour et al. (Equations (5) and (6)) show conservative results compared to results from Sharma's equation (Equation (2)). This may have occurred due to the former three equations considering explicitly the parameters affecting the shear strength of SFRC beams. By contrast, Sharma's model misses the effects of longitudinal reinforcement ratio and steel fiber parameters. By using Equations (3) and (5), most of the data appears above the lower dashed line; by contrast, using the second equation of Ashour et al. (Equation (6)) exhibits more data appearing below the bottom dashed line (Figure 3d) compared to results from Equations (3) and (5).

Parra-Montesinos [15] constructed a database by considering the shear span-to-effective depth ratio, cylinder concrete compressive strength, fiber volume fraction, steel fiber tensile strength, and fiber aspect ratio. Parra-Montesinos [15] set $0.3\sqrt{f'_c}$ (Equation (7)) as a lower bound for evaluating the application of steel fibers in SFRC beams and for supporting the use of deformed steel fibers as the minimum shear reinforcement regardless of the shear span-to-effective depth ratio, concrete compressive strength, or the longitudinal tensile reinforcement ratio. Parra-Montesinos [15] reported that the shear stress values of SFRC beams with fiber volume fraction of 0.75% or greater (based on Parra-Montesinos's database) were greater than $0.3\sqrt{f'_c}$ (MPa). Figure 3e shows that there are 60 specimens located below the lower dashed line. In general, the shear strength model from Parra-Montesinos (Equation (7)) is more conservative than that derived by Sharma (Equation (2)).

The equation proposed by Kwak et al. (Equation (8)) appears to be superior to the equations proposed by Sharma (Equation (2)), Narayanan and Darwish (Equation (3)), and Ashour et al. (Equation (5)). Only 18 points appear below the lower dashed line. This number is slightly greater than the number exhibited by using Equation (6). The shear model proposed by Kwak et al. involves the important parameters affecting shear strength. Dinh's shear strength model is not as conservative as the shear strength model proposed by Kwak et al., since the former has 131 specimens appearing above the upper dashed line, while the latter shows 137 specimens appearing above the upper dashed line. Wu's shear strength model is similar to Dinh's shear strength model; however, the latter shows better results. Using Wu's equation leads 32 specimens to lie below the bottom dashed line, while Dinh's equation results in 30 specimens lying below the bottom dashed line. Among the eight equations reviewed, the shear strength prediction equation proposed by Narayan and Darwish (Equation (3)) [12] shows the smallest coefficient of variation (COV). Therefore, out of these eight equations, Equation (3) can show more precise results.

3. Experimental Program

The purpose of the experimental program is to verify the shear strength prediction equations collected in this study. Ten SFRC specimens were prepared. A detailed experimental program is shown in the next three sub-chapters.

3.1. Specimen Design

The specimens were divided into two series, designated as B1 and B2. There were 6 beams for series B1 and 4 beams for series B2. The beams were tested up to failure, in order to evaluate the effects of shear span-to-effective depth ratio and longitudinal tensile reinforcement ratio, and to verify the proposed equation. Those varied parameters were selected because the shear span-to-effective depth and longitudinal tensile reinforcement ratios were superior to other parameters in affecting the shear strength of SFRC beam. Moreover, the shear-span-to-effective depth ratios were selected in such way that the specimens were classified as specimens with short to long shear spans. In the case of a specimen with intermediate shear span-to-effective depth ratio, the failure mode can be either shear failure or flexural failure.

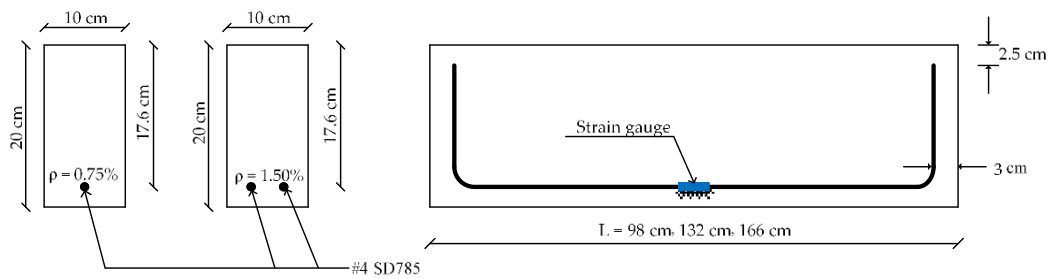
Table 2 shows the details of specimen design. The beams in series B1 that had a section size of 100 mm × 200 mm were divided into three types on the basis of their length. The beam lengths of 980 mm, 1320 mm, and 1660 mm corresponded with shear span-to-effective depth ratios of 2, 3, and 4, respectively. Every beam in series B1 was reinforced longitudinally by using a longitudinal bar with a diameter of 13 mm (#4). Also, each beam of each length in series B1 had two types of longitudinal reinforcing bar ratios, that amounted to 0.75% and 1.5%. The first ID denotes the series number with the two numbers following the series number denoting the shear span-to-effective depth and longitudinal reinforcement ratios. For beams in series B2, the section size for all beams tested was 100 mm × 250 mm and the beams were divided into two types on the basis of their length. The lengths of 1480 mm and 1700 mm corresponded with shear span-to-effective depth ratios of 2.5 and 3, respectively. A longitudinal bar with a diameter of 25.4 mm (#8) was provided for each beam in series B2. The first ID in series B2 show the series number and is followed by three numbers. The first, second and third numbers following the series ID are the shear-span-to-effective depth ratio, the longitudinal reinforcement ratio, and the specimen number, respectively. It is worth mentioning that there are two specimens for each shear span-to-effective depth ratio.

Table 2. Details of specimen design.

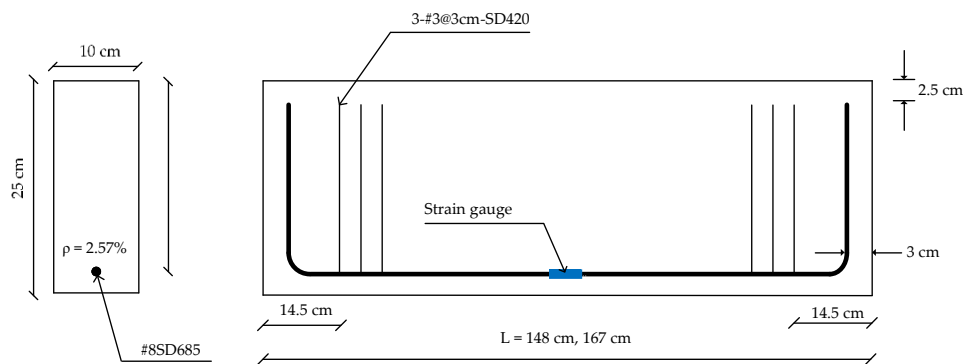
Specimen ID	b (mm)	h (mm)	d (mm)	L (mm)	Longitudinal Reinforcing			Steel Fibers			
					$f_{y,specified}$ (MPa)	ρ (%)	n-Size	V_f (%)	L_f (mm)	D_f (mm)	$f_{su,SF}$ (MPa)
B1-2-0.75	100	200	176.35	980	785	0.75	1-#4	1.5	30	0.38	2300
B1-3-0.75				1320							
B1-4-0.75				1660							
B1-2-1.5				980							
B1-3-1.5				1320							
B1-4-1.5				1660							
B2-2.5-2.5-1	100	250	197.3	1480	685	2.5	1-#8	1.5	30	0.38	2300
B2-2.5-2.5-2				1700							
B2-3-2.5-1											
B2-3-2.5-2											

No stirrups were provided for both series, so the high-strength hooked-end steel fibers with a fiber volume fraction of 1.5% were used instead. It is noteworthy that the fiber volume fraction or fiber volume ratio is defined as the fiber volume percentage in the entire volume of a fiber reinforced concrete. The longitudinal reinforcing bars were extended over the supports, hooked upward, and enclosed

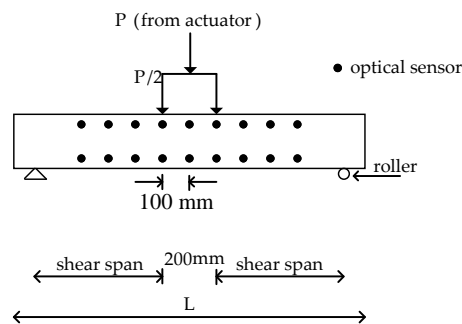
with stirrups with diameter of 10 mm and yield stress of 420 MPa in each end of each beam. Figure 4 shows the details of specimens.



(a) Beam specimens in series B1



(b) Beam specimens of series B2



(c) Test setup



(d) Selected beam specimen subjected to two point vertical loads

Figure 4. Specimen design, test setup and configuration of instruments, and a beam subjected to monotonic two point vertical loads.

3.2. Materials

The designed concrete compressive strength was 70 MPa. The concrete specimens were made of ASTM type I Portland cement, granulated blast furnace slag (GGBS), fly ash (series B1), silica fume (series B2), coarse aggregates with a nominal maximum size of 19.05 mm (series B1) and 9.5 mm (series B2), natural river sands as fine aggregate with fineness modulus of 2.8, and superplasticizer, which was used to improve the workability of fresh concrete. The longitudinal reinforcement was high-strength reinforcing bars with specified yield strength of 685 MPa and 785 MPa for bars #8 and #4, respectively. Furthermore, the steel fibers were high-strength, hooked-end steel fibers with an ultimate tensile strength of 2300 MPa, a diameter of 0.38 mm, a length of 30 mm, a specific gravity of 7.85, and an elastic modulus of 200 GPa. Table 3 presents two mix proportions for series B1 and B2. The weight of steel fibers in 1 m³ of concrete is determined by multiplying fiber volume fraction with density of steel fibers.

Table 3. Details of mix proportions (kg/m³).

Series	Cement	GGBS	Fly Ash	Silica Fume	Sand	Coarse Aggregate	Water	SP	Steel Fibers
B1	373	203	102	-	993	462	230	5	118
B2	372	255	-	50	1000	400	215	9.3	118

3.3. Test Setup

Along with each beam, control cylinders were prepared. Compression tests were conducted on 100 × 200 mm cylindrical specimens according to ASTM C39. A servo-hydraulic, closed-loop testing machine with a capacity of 1000 kN applying a monotonically increasing displacement loading with a constant rate of 0.01 mm/s performed compression tests on concrete cylinders. This machine was also used to perform tensile tests on longitudinal bars in order to measure yield and ultimate stress. The beam specimen testing arrangement is shown in Figure 4. Two concentrated loads were applied at the top of the beam specimens. The beam tests were performed with a servo-hydraulic, closed-loop testing machine with a capacity of 5000 kN and a displacement rate of 0.01 mm/s. The beams were supported by a hinge on one end and roller at the other. In order to record specimen deformation, an optical motion tracking system was used to detect the movement of 18 optical sensors attached on specimens, as shown in Figure 4c. The selected beam specimen experiencing bending test is shown in Figure 4d.

4. Experimental Results

4.1. Material Test Results

Tables 4 and 5 show the test results from the compression tests of concrete cylinders and the tensile tests on reinforcing bars, respectively. The compression tests were performed on the same day with testing specimens. It can be seen that concrete cylinders corresponding to specimens B1 had compressive strength greater than 70 MPa. For concrete cylinders corresponding to B2, it showed that these concrete compressive strengths were slightly less than 70 MPa. The tensile test results show that bars with diameters of 13 mm and 25 mm had yield stresses larger than their specified yield stresses.

Table 4. Compression test results for concrete cylinders.

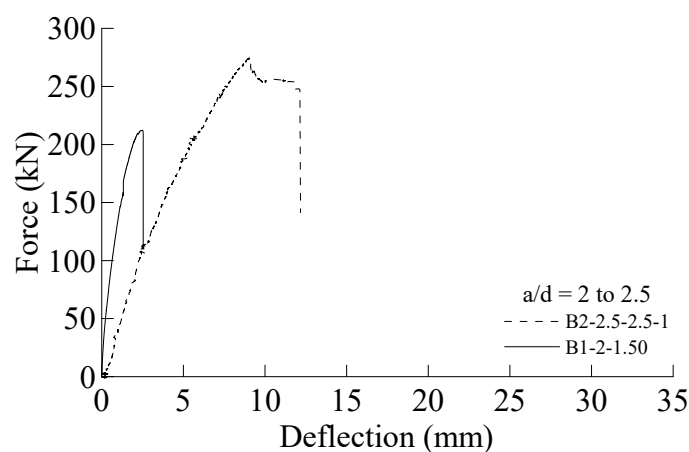
Specimen ID	Concrete Compressive Stress (MPa)
B1-2-0.75, B1-2-1.50 B1-3-0.75, B1-3-1.5	82.4
B1-4-0.75, B1-4-1.5	78.2
B2-2.5-2.5-1, B2-2.5-2.5-2	61.5
B2-3-2.5-1, B2-3-2.5-2	62.4

Table 5. Tensile test results for reinforcing bars.

Reinforcing Bar Size (Diameter [mm])	Specified Yield Stress (MPa)	Test Results (MPa)	
		Yield Stress	Ultimate Stress
#4 (12.7 mm)	785	785	978
#8 (25.4 mm)	685	703	907

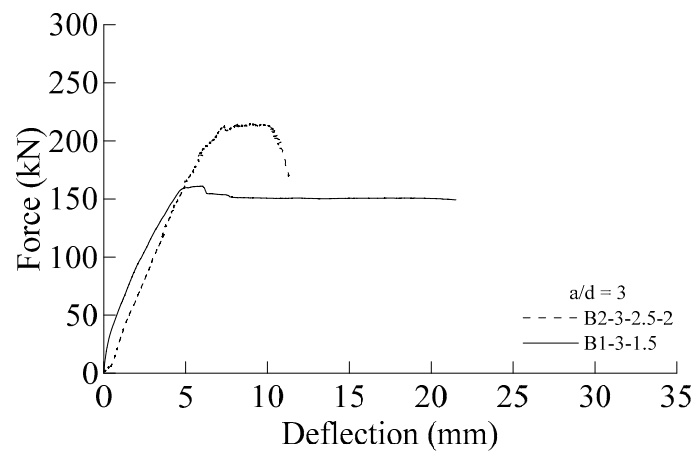
4.2. Specimen Failure

The total vertical load-midspan deflection relationship for selected specimens is presented in Figure 5. Figure 6 shows the final appearance of all specimens. Almost all beams in series B1 failed in flexural followed by shear (flexural-shear failure), except B1-2-1.5. The specimen B1-2-1.5 showed arch action instead of beam action. The inclined cracking in specimen B1-2-1.5 claimed that the load was transferred directly to the support through compression strut. Therefore, the failure mode of specimen B1-2-1.5 was compression strut failure. For the beam failing in flexural or flexural-shear, the strain gauge attached on a longitudinal reinforcing bar proved that the yield strain occurred when the peak strength of a specimen was reached. In general, flexural and shear cracks appeared and the crack opening at the middle of beam gradually increased as the vertical load increased. It can be seen in Figure 6, that the beams of series B1 (except B1-4-1.5) showed cracks around the concentrated load. Specimen B1-4-1.5 showed a horizontal crack and a vertical crack that opened gradually at the middle of the specimen. The failure mode of specimen B1-4-1.5-1 consisted of flexural-shear and bond splitting failures.

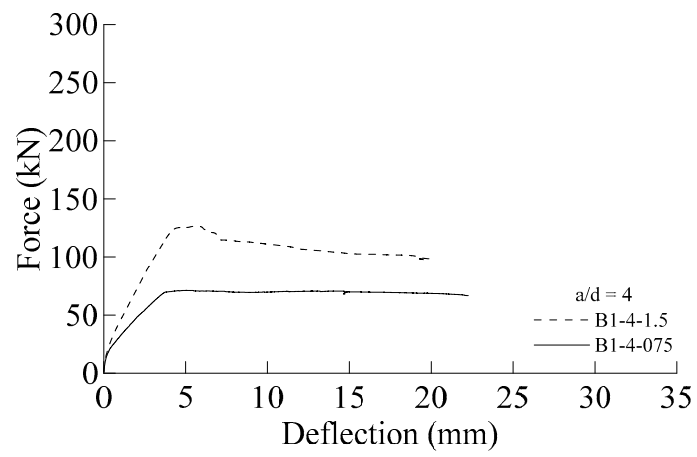


(a) a/d of 2 and 2.5

Figure 5. Cont.



(b) a/d of 3



(c) a/d of 4

Figure 5. The force-middle span deflection curves for selected specimens.



(a) B1-2-0.75



(b) B1-2-1.5



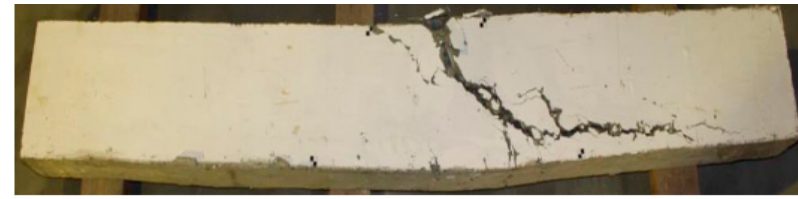
(c) B1-3-0.75



(d) B1-3-1.5



(e) B1-4-0.75



(f) B1-4-1.50



(g) B2-2.5-2.5-1



(h) B2-2.5-2.5-2

Figure 6. The final appearance of beam specimens at the end of tests.

Specimens series B2 consisted of 4 SFRC beams. Three of four specimens failed in shear. The failure mode of B2-3-2.5-1 was a combination of compression failure due to flexural and web crushing, where yielding of the longitudinal reinforcing bars occurred. For beam B2-2.5-2.5-1, the diagonal cracks appeared as the load gradually increased. Small flexural cracks also appeared. A large diagonal crack and horizontal crack appeared on one of the shear spans, followed by the crushing of concrete directly at the top of the beam (around the concentrated load). These failure modes show that beam B2-2.5-2.5-1 had a combination of diagonal tension and shear compression failures. For beam B2-2.5-2.5-2, the diagonal cracks appeared as the load gradually increased. The crushing of concrete occurring around the concentrated load and large diagonal crack in one of shear spans occurred simultaneously. The final appearance of beam B2-2.5-2.5-2 shows that the beam failed due to a combination of diagonal tension and shear compression failures. For beam B2-3-2.5-1, cracks started appearing from the middle of both shear spans (left and right shear spans); it then propagated to the middle span around the concentrated loads. Cracks on the middle span became larger, and crushing of concrete at the top of beam occurred. In addition, it was found that yielding of the longitudinal reinforcement occurred in specimen B2-3-2.5-1. Therefore, beam B2-3-2.5-1 failed due to web shear crushing and flexural failure. Beam B2-3-2.5-2 failed due to diagonal tension and shear compression failures. As the vertical load gradually increased, cracks appeared on both shear spans. Cracks tended to propagate to the middle span around concentrated loads. The crushing of concrete at the top of the beam occurred first, and width of diagonal crack became larger accordingly.

In general, based on the failure modes, a beam with shear-span-to-effective depth ratio of 2 to 2.5 refers to beam with a short shear span-to-effective depth ratio, and the most failure mode is shear failure. For a beam with a shear-span-to-effective depth ratio of 4, the failure mode expected is flexure or flexure-shear failure. In addition, this beam can be classified as a beam with long shear-span-to-effective depth ratio. Meanwhile, two possibilities of failure mode can occur in beams with a shear span-to-effective depth ratio of 3. As mentioned, two beams with a shear span-to-effective depth ratio of 3 showed different failure modes. According to the failure modes, this study indicates that the minimum shear span-to-effective depth ratio for a flexural member is 3.

4.3. Ultimate Shear Strength

The shear strengths corresponding to nominal flexural strength, the test results for SFRC beams, and the predicted shear strengths based on previous shear strength prediction models are summarized in Table 6. The shear strength a specimen was defined as half of the maximum force ($V_{c,test} = 0.5P_{u,max}$). The symbol $P_{u,max}$ denotes the maximum of vertical load applied by the vertical actuator, while the symbol $V_{n,f}^*$ stands for the shear strength corresponding to flexural strength. The effect of shear span-to-effective depth and longitudinal tensile reinforcement ratios can be observed from beam B1. For beam B2, only the effect of shear span-to-effective depth ratio was observed. Moreover, the mean and COV values for measured-to-predicted strengths are shown in Table 6.

From beams B1 with a longitudinal reinforcement ratio of 0.75%, the shear strength of beams B1-2-0.75, B1-3-0.75, and beams B1-4-0.75 were 72.6 kN, 46.50 kN, and 35.70 kN, respectively. For series B1 with a longitudinal reinforcement ratio of 0.75%, the decrease of the ultimate shear stress due to the change of the shear span-to-effective depth ratio from 2 to 3, and 3 to 4 were about 36% and 23%, respectively. In series B1, with a longitudinal reinforcement ratio of 1.50%, the ultimate shear strength decrease was about 24% when the shear span-to-effective depth ratio increased from 2 to 3, and the shear span-to-effective depth ratio increasing from 3 to 4 led the shear strength to decrease by about 21%. In addition, improving the longitudinal tensile reinforcement ratio increased ultimate shear strength by about 46%, 73%, and 71% for beams with span-to-effective depth ratios of 2, 3, and 4, respectively. From series B2, the improvement of the shear span-to-effective depth ratio from 2.5 to 3 decreased ultimate shear strength by about 12%.

Table 6. Comparison between measured and predicted strengths.

Specimen ID	$V_{n,f}$ (kN)	$V_{c,test}$ (kN)	Predicted Shear Strengths (kN)							
			Sharma (1986)	Narayanan and Darwish (1987)	Ashour et al. (1992)		Parra-Montesinos (2006)	Kwak et al. (2002)	Dinh (2009)	Wu (2014)
					Equation (5a)	Equation (6)				
B1-2-0.75	60.71	72.6	70.90	71.41	28.49	67.62	48.02	57.31	39.58	70.84
B1-2-1.50	104.15	106.1	70.90	78.84	35.89	68.76	48.02	64.81	49.18	78.83
B1-3-0.75	40.48	46.50	64.06	59.40	24.89	45.08	48.02	53.66	39.58	70.84
B1-3-1.50	69.43	80.50	64.06	62.93	31.35	45.84	48.02	60.21	49.18	78.83
B1-4-0.75	30.17	35.70	58.08	57.48	22.27	33.09	46.78	50.57	39.37	69.44
B1-4-1.50	51.72	63.30	58.08	60.13	28.05	33.66	46.78	56.32	48.76	77.16
B2-2.5-2.5-1	114.81	120.55	64.81	76.93	40.87	56.16	46.42	68.96	59.30	92.10
B2-2.5-2.5-2	114.81	114.63	64.81	76.93	40.87	56.16	46.42	68.96	59.30	92.10
B2-3-2.5-1	97.09	95.10	62.37	70.49	38.62	47.06	46.76	67.11	59.78	92.95
B2-3-2.5-2	97.09	114.63	62.37	70.49	38.62	47.06	46.76	67.11	59.78	92.95
Mean of $V_{c,test}/V_{c,predicted}$			1.32	1.21	2.50	1.70	1.80	1.35	1.65	1.02
COV			0.34	0.28	0.19	0.29	0.36	0.27	0.25	0.28

In general, the test results present the effect of the shear span-to-effective depth ratio and the longitudinal tensile reinforcement ratio, as shown in Figures 1 and 2. According to Figure 1, increasing the shear span-to-effective depth ratio decreases the normalized ultimate shear strength by 14 to 24%. Therefore, the trend showing the decrease of ultimate shear strength with the increase of shear-span-to-effective depth ratio shown in Figure 1 agrees with the experimental results. Figure 2 shows the effect of the longitudinal tensile reinforcement ratio on the SFRC beam shear strength. It shows that improving the longitudinal tensile reinforcement ratio may increase the ultimate shear strength by approximately 60% or more. This agrees with the improvement of the shear strength from improving the longitudinal tensile reinforcement ratio that has been shown in this study. Furthermore, it can be known that the presence of the high longitudinal reinforcement ratio tends to decrease the rate of decrease of shear strength due to the increase of shear span-to-effective depth ratio.

No effect of yield strength of longitudinal reinforcement was observed in the experimental program in this study. However, it can be predicted that varying the yield strength of longitudinal bar has no effect on shear strength of a normal reinforced concrete or SFRC beam that is designed to fail in shear.

5. Comparison between Measured Shear Strength and Shear Strength Corresponding to Nominal Flexural Strength

The shear corresponding to the flexural capacity of each beam is presented. The nominal flexural strength was calculated based on ACI ITG-4.3R-07 [40], and the tension stress of beam due to the presence of steel fibers was considered as well. By referring to research conducted by Naaman [41], the strain and stress distribution and internal force acting on the SFRC beam section are shown in Figure 7. The rectangular stress block is used for compression zone, while the nonlinear distribution starting from maximum tensile stress (σ_{pc}) near the neutral axis to minimum value at the extreme tension fiber is the actual tensile stress [41]. For simplification, the tensile stress distribution can be assumed as an inverse triangle with the maximum tensile stress on the neutral axis [41]. For any RC beams, the cracks appear at the extreme tension fiber first and continue developing from the extreme tension fiber to upper parts in tension zone. Therefore, it is acceptable to define the maximum tensile stress to be near the neutral axis and the smallest tensile stress to be at the extreme tension fiber.

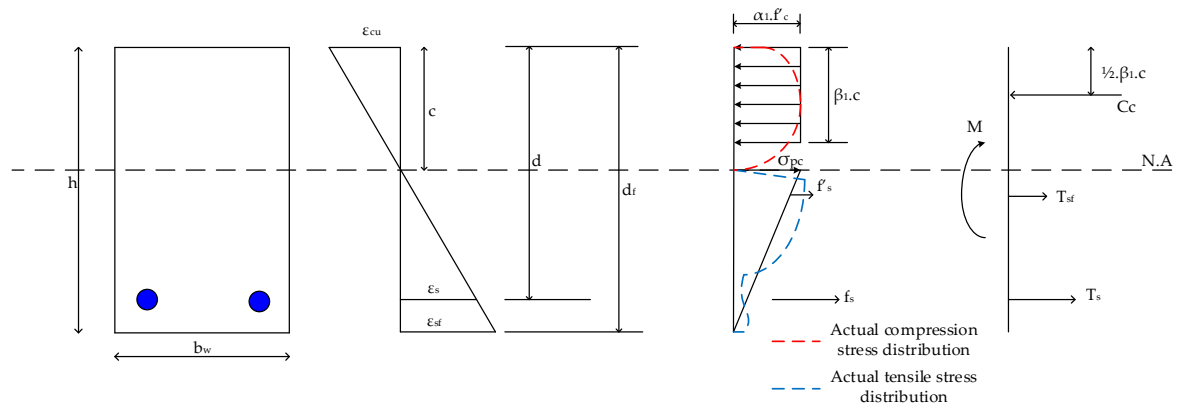


Figure 7. General strain, idealized stress distribution, and internal force of steel fiber-reinforced concrete (SFRC) beam section [41].

As mentioned in ACI Committee 544 [42] and reported by Wu [28], the compressive strain at the extreme layer of the compression zone ranged from 0.0035 to 0.004. Since the depth of the neutral axis is still unknown, the first key step in section analysis is to accomplish section equilibrium. Therefore, by assuming the beam to be only subjected to the bending (with axial force of zero), the sum of the compression force can be set to be equal to the sum of the tension force, as shown in Equation (13). Solving Equation (13) can be based on a trial and error procedure in order to determine the depth of the neutral axis. The nominal moment strength is expressed as the sum of the tension force multiplied by the moment arm, as shown in Equation (14).

For all series B1, the shear strength corresponding to the flexural strength is less than the measured shear strength. By contrast, for all series B2, the measured strength tended to be similar to shear strength corresponding to flexural strength. Figure 6 shows that three out of four beams in series B2 experienced shear failure. The horizontal crack near support and the diagonal cracks from the middle of shear span to the top of the beam around the concentrated load could be discerned. Only specimen B2-3-2.5-1 failed due to the combination of flexural and web-crushing with yielding of the longitudinal reinforcing bar. By referring to flexural analysis, the compression force acting on the top of the beam due to bending might contribute to produce crushing of concrete on the top of the beams. Therefore, the shear failure and compression failure due to bending might occur simultaneously.

$$C_c = T_s + T_{SF} \tag{13}$$

$$\text{or } \alpha_1 f'_c b \beta_1 c = A_s f_s + \sigma_{pc} b (h - c)/2$$

$$M_n = T_s \left(d - \frac{1}{2} \beta_1 c \right) + T_{SF} \left(\frac{1}{3} (h - c) + \left(c - \frac{1}{2} \beta_1 c \right) \right) \tag{14}$$

6. Comparison between Experimental and Predicted Results

The measured ultimate shear strengths were verified using shear prediction equations presented in this study. For beams of series B1 with a shear span-to-effective depth of 2, the measured shear strengths were greater than the shear strengths predicted by using equations summarized in this study. On the other hand, the measured shear strengths of series B1 with 3 and 4 and a longitudinal reinforcement ratio of 0.75% were less than the predicted shear strengths proposed by Sharma (1986), Narayanan and Darwish (1987), and Kwak et al. (2002), Parra-Montesinos (2006), and Wu (2014). In contrast, the equation proposed by Dinh (2011) exhibited a result that was slightly less than the measured shear strength for specimen B1-1-0.75. In addition, the shear strength equation proposed by Wu (2014) slightly overestimated the shear strength of specimen B1-4-1.5. For specimens in series B1, the comparison between measured and predicted strengths showed that most equations overestimated the shear strength of SFRC beam specimens, while only both equations proposed by Ashour et al.

(1992) gave results smaller than test results. Among specimens B1, only specimen B1-2-1.5 failed in shear. For series B2, all strengths obtained by using shear strength equations reviewed in this study were less than those obtained from the experimental program.

It can be expected that the shear strength prediction equations proposed by previous researchers were developed by using their own test results or a beam database dominated by beam specimens failing in shear. Therefore, for a specimen with flexural or flexural-shear failure, it is absolutely normal if the predicted shear strength is greater than the measured shear strength. Meanwhile, as shown in Table 6, only the Equation (11) could give results closer to the test results of series B2. In general, Equation (11) can show more precise and reasonable results compared to the other reviewed equations. The mean and COV values exhibited by using Equation (11) are 1.02 and 0.28, respectively.

7. Proposed Prediction Equations

Based on the test results summarized in Table 6, only the shear strength model proposed by Wu in 2014 (Equation (11)), tends to be closer to the test results of series B2 compared to other proposed equations. The predicted results obtained by using Equation (11) are more precise and reasonable than the predicted results obtained by other researchers. However, based on examination of shear strength equations by using the shear strength database, Equation (11) is not as accurate as Equation (3). This is because the former exhibits the mean and COV of 1.43 and 0.58, respectively, while the latter shows the mean and COV of 1.27 and 0.35, respectively. The inability and inconsistency of previous equations in predicting the shear strength of SFRC beams prove that the need for a reliable equation to predict the shear strength of SFRC beams must be realized. Moreover, besides the agreement between the test and the predicted results, all previous prediction equations are still expressed as the summation of concrete contribution and steel fiber contribution. No study clearly presented the real mechanism of steel fibers in concrete nor expressed the steel-fiber and concrete beam parameters as one term. However, combining steel-fiber and RC beam parameters in one term can be assumed to be acceptable, since the steel fibers are also part of the materials in the SFRC beam, and it can only be expected that there must be an interaction between steel fibers and concrete.

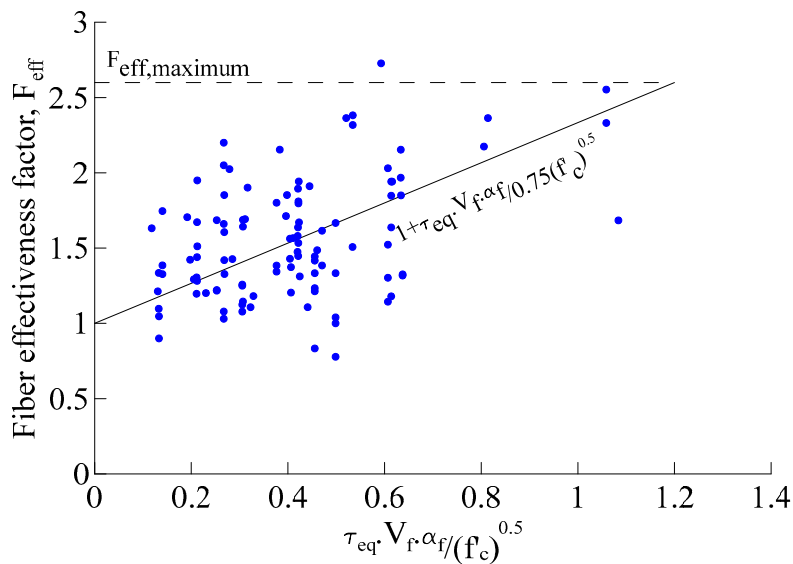
In this study, the prediction equation for SFRC beams is proposed by expressing the concrete and steel fiber parameters in one term. Also, the prediction equation is proposed such that in the absence of steel fibers, the equation is applicable to reinforced concrete beam without the steel fibers. Therefore, the prediction equation is expressed as the multiplication between the shear strength equation for normal RC beams and fiber effectiveness factor. The ACI 318-14 detailed equation for prediction shear strength [5] is adopted in this study, since this equation is a function of the tensile longitudinal reinforcement ratio, the shear span-to-effective depth ratio, and the square-root of concrete strength. In addition, the detailed shear strength equations provided in ACI 318-14 or older versions were developed based on the analysis reported in the ACI-ASCE Committee 326 report [5,43], where the discussed failure modes were shear and diagonal tension. Therefore, developing the proposed equation for SFRC beams from an equation derived based on shear and diagonal tension is reasonable.

The fiber effectiveness factor must contain the fiber aspect ratio, the fiber volume fraction, the bond strength along fiber-matrix interface, and the concrete strength. The relationship between ratios of shear stress of SFRC beam specimen-to-plain concrete beam (control specimen) and ratios of multiplication among the fiber aspect ratio, the fiber volume fraction, the bond strength along fiber-matrix interface to square-root of concrete strength are presented in Figure 8, in which the fiber effectiveness factor equation is derived through regression analysis. Based on test results summarized in Table A1, it is noteworthy that some authors only showed the shear strengths of SFRC beams without providing the shear strengths of plain concrete beams. Therefore, only 107 test results are involved in Figure 8a. Figure 8b shows the comparison between ratios of shear stress of SFRC beam specimen-to-plain concrete beam (control specimen) and predicted fiber effectiveness factors. The proposed equation is

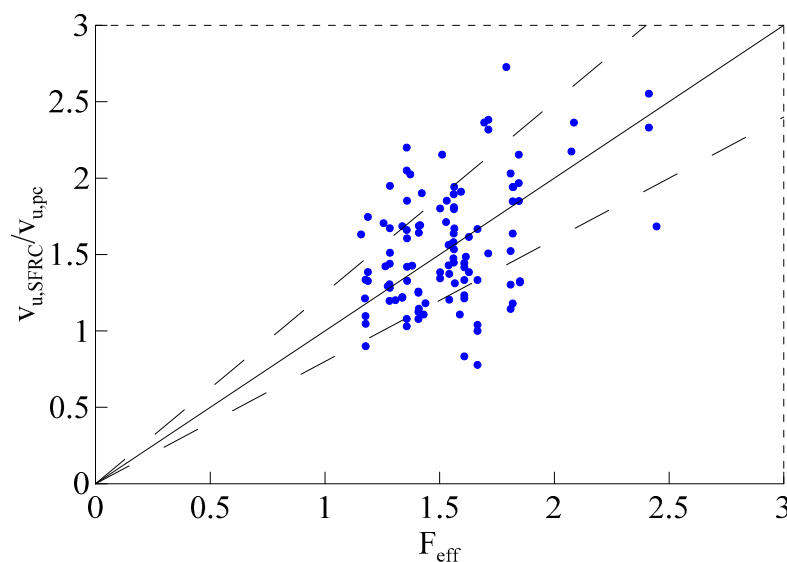
given in Equation (16), that was proposed such that only few data appear below the bottom dashed line in Figure 8b. This may lead the prediction equation to give a conservative result.

$$V_{c,SF} = \left(0.16 \sqrt{f'_c} + 17.2\rho_w \frac{V_u d}{M_u}\right) F_{eff} b_w d \tag{15}$$

$$, \text{ where } F_{eff} = 1 + \frac{\tau_{eq} V_f \frac{L_f}{d_f}}{0.75 \sqrt{f'_c}} \tag{16}$$



(a) The relationship between between $V_{c,SFRC}/V_{c,pc}$ and steel fiber parameter



(b) Comparison between $V_{c,SFRC}/V_{c,pc}$ and fiber effectiveness factor

Figure 8. Proposed fiber effectiveness factor equation and comparison between SFRC shear strength-to-normal concrete shear strength ratios and proposed fiber effectiveness factor.

Figure 9 shows the relationship between the normalized shear strength and multiplication between the tensile longitudinal reinforcement ratios and the ratios of shear-span-to-effective depth divided

by the square-root of concrete strength $\left(\rho \cdot \frac{V_u d}{M \sqrt{f'_c}}\right)$. The upper bound for SFRC beam is proposed as multiplication between $0.29 \sqrt{f'_c}$ (MPa) and the fiber effectiveness factor instead of setting the value to be nearer the average value given by test data. This consideration is based on the limitation of the SFRC beam database, where no test data with a higher value of $\left(\rho \cdot \frac{V_u d}{M \sqrt{f'_c}}\right)$ appeared. Therefore, in the absence of steel fibers, the limit of concrete stress remains equal to $0.29 \sqrt{f'_c}$ (MPa), as set in ACI 318-14 and previous ACI 318 codes. Using the shear stress of RC $0.29 \sqrt{f'_c}$ (MPa) also reconfirms test data constructed by Parra-Montesinos [15], that set the lower bound shear stress as $0.30 \sqrt{f'_c}$ (MPa) for SFRC beam design.

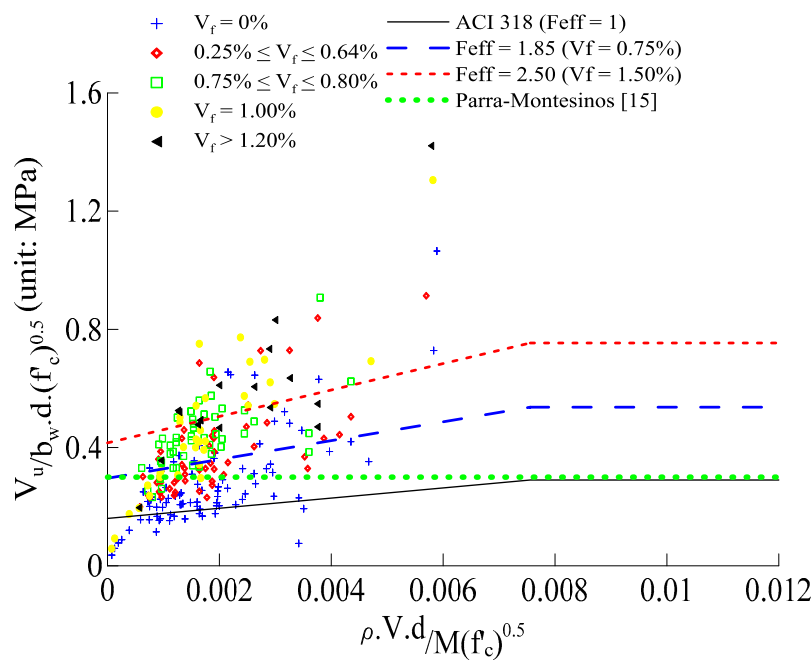


Figure 9. The relationship normalized beam shear strengths and beam parameters.

The proposed shear strength equation is given in Equation (17). Two lines corresponding to the fiber volume fraction of 0.75% and 1.50% are shown as well. The upper limit of 0.3 in. dashed line, that corresponds to fiber effectiveness factor for fiber volume fraction of 0.75%, is only passed by few data points, which correspond with specimens with fiber volume fraction in the range of 0.75% to 0.80%. Meanwhile, only two data points with a fiber volume fraction of 1.50% pass the upper limit of 0.1 in. dashed line, that corresponds to the fiber effectiveness factor for the fiber volume fraction of 1.50%. For practical application, it is highly recommended to use a fiber volume fraction of not greater than 1.50%. According to Liao et al. in 2017 and Perceka in 2019 [44], the SFRC material needs fiber volume fraction to be less than 2% to meet tensile strain hardening criteria. With tensile strain hardening behavior, a loaded SFRC member experiencing bending moment and shear has more resistance to crack opening, can avoid strain localization, and improve energy absorbing capability through showing multiple cracks on its surface. Furthermore, the fiber effectiveness factor shall not exceed 2.6. The maximum number of the fiber effectiveness factor is taken based on the nearest number to the largest value, shown in Figure 8a.

$$V_{c,SF} = \left(0.16 \sqrt{f'_c} + 17.2 \rho_w \frac{V_u d}{M_u}\right) F_{eff} b_w d \leq 0.29 \sqrt{f'_c} F_{eff} b_w d \quad (17)$$

8. Evaluation of Proposed Shear Strength Prediction Equation

Equation (17) is verified by using 236 test results. The relationship between the test results of 236 beams and the predicted results based on the proposed prediction equations is shown in Figure 10. The number of data appearing below the bottom dashed line is less than 13, while there are 151 test results appearing above the upper dashed line. Also, compared to Equation (3), using the proposed prediction equation results in little loss of accuracy of about 11.43 percent, where Equations (3) and (17) corresponds with COV of 0.35 and 0.39, respectively. With mean values obtained by using Equations (3) and (17) corresponding with 1.27 and 1.44, respectively, it can be proven that the proposed equation is more conservative than Equation (3). Table 7 shows the comparison between the shear strength of beam specimens tested and the shear strengths calculated by using Equation (17). For the beams of series B1, specimens B1 with a/d of 3 with longitudinal reinforcement ratio of 0.75% and a/d of 4 with longitudinal reinforcement ratios of 0.75% and 1.50% show that the measured shear strengths were less than the predicted shear strengths. Compared with the shear strengths of series B2, the ones obtained by using the proposed prediction equation shows lower results. The mean and COV obtained by using Equation (17) are 1.14 and 0.30, respectively.

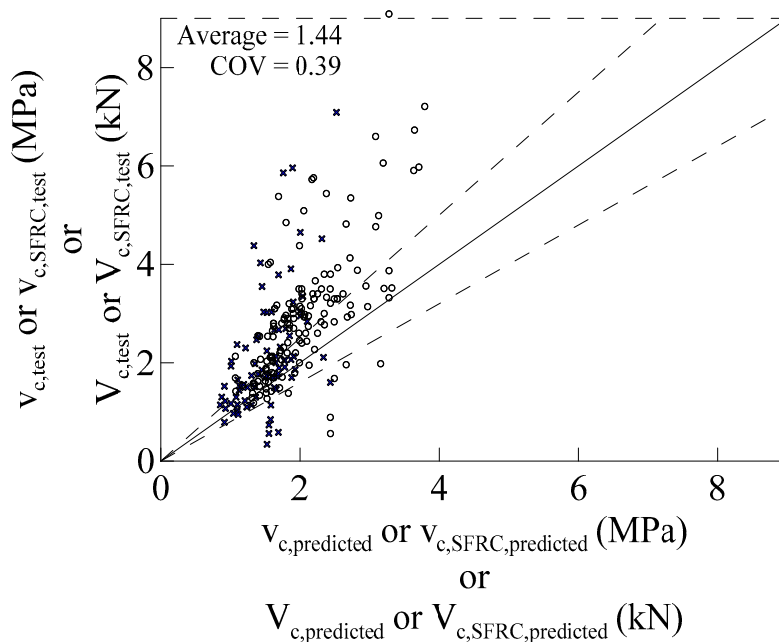


Figure 10. Comparison between experimental and proposed prediction results (Equation (17)).

Table 7. Comparison between measured and predicted strengths.

Specimen ID	$V_{n,f}$ (kN)	$V_{c,test}$ (kN)	$V_{c,proposed}$ (kN)	$V_{c,(Equation18a\ or\ Equation19)}$ (kN)	$V_{c,(Equation18b\ or\ Equation19)}$ (kN)
B1-2-0.75	60.71	72.6	70.75	69.09	52.56
B1-2-1.50	104.15	106.1	76.48	69.09	66.23
B1-3-0.75	40.48	46.50	67.89	69.09	52.56
B1-3-1.50	69.43	80.50	70.75	69.09	66.23
B1-4-0.75	30.17	35.70	65.57	67.63	51.45
B1-4-1.50	51.72	63.30	67.49	67.63	64.83
B2-2.5-1	114.81	120.55	79.30	68.39	78.34
B2-2.5-2	114.81	114.63	79.30	68.39	78.34
B2-3-1	97.09	95.10	76.03	68.89	78.91
B2-3-2	97.09	114.63	76.03	68.89	78.91
Mean of $V_{c,test}/V_{c,predicted}$			1.14	1.24	1.24
COV			0.30	0.35	0.24

The evaluation results show that the proposed shear strength prediction equation can be applied to predict the shear strength of RC or SFRC beams with a concrete compressive strength, fiber volume fraction, yield strength of longitudinal reinforcing bar, and shear-span-to-effective depth ratio ranging from 20 MPa to 194 MPa, 0% to 1.5%, 420 MPa to 785 MPa, and 2.5 to 6.0. The shear strength of a beam with shear-span-to-effective depth ratio less than 2.5, particularly a beam without steel fibers, shall be calculated or predicted by using other methods, since that beam is classified as deep beam and has different behavior with beams tested in this study.

9. Examination of Shear Strength Equation Provided in ACI 318-19 Code

According to ACI 318-19 [45], the shear strength of non-prestressed members is a function of concrete strength, axial load acting on section, size effect, section area, effective depth, member width, and longitudinal reinforcement ratio. In ACI 318-19, Equations (18a) and (18b) are the equations for calculating the shear strength of RC members containing the shear reinforcement greater than the minimum shear reinforcement. For other cases, Equation (19) shall be used. The parameter λ_s is the size modification factor that shall be determined by Equation (20), in which the effective depth of beam to determine λ_s shall be expressed in inch unit.

$$V_{c,SF} = \left(0.17 \sqrt{f'_c} + \frac{N_u}{6A_g}\right) F_{\text{eff}} b_w d \quad (18a)$$

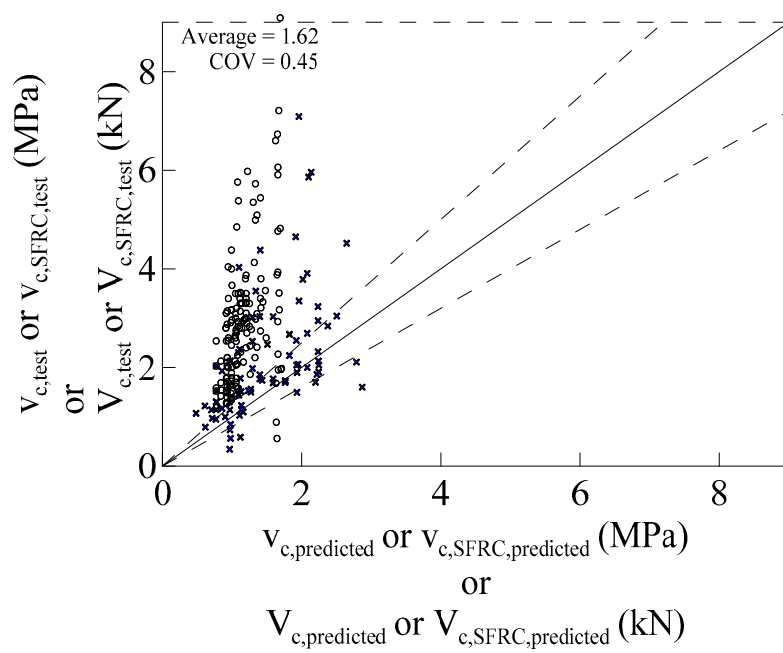
$$V_{c,SF} = \left(0.66(\rho_w)^{\frac{1}{3}} \sqrt{f'_c} + \frac{N_u}{6A_g}\right) F_{\text{eff}} b_w d \quad (18b)$$

$$V_{c,SF} = \left(0.66\lambda_s(\rho_w)^{\frac{1}{3}} \sqrt{f'_c} + \frac{N_u}{6A_g}\right) F_{\text{eff}} b_w d \quad (19)$$

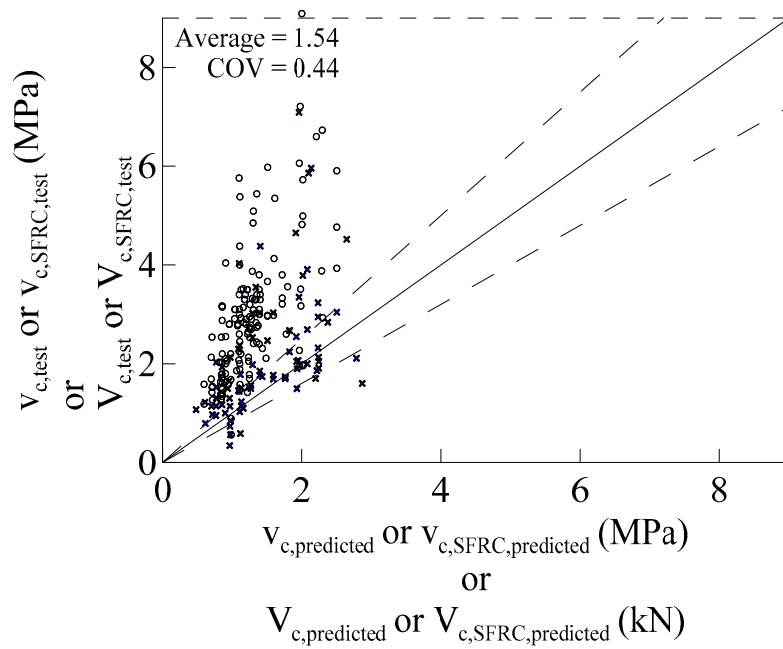
$$\lambda_s = \sqrt{\frac{2}{1 + \frac{d}{10}}} \quad (20)$$

Due to the absence of shear reinforcing bars in this study, the SFRC beam with a fiber volume fraction of 0.75% or greater is classified as a RC beam with minimum shear reinforcement; otherwise, SFRC beams are classified as RC beams with the shear reinforcement less than the minimum shear reinforcement. Multiplying Equation (18) or (19) with the fiber effectiveness factor is performed to examine the applicability of the shear strength equation provided in ACI 318-19 as the basic equation for predicting the shear strength of SFRC beam.

The relationship between measured strengths and predicted shear strengths using the multiplication between ACI 318-19 and the fiber effectiveness factor is shown in Figure 11. The shear strength database is used to evaluate the accuracy of the equations. The predicted shear strength shown in Figure 11a is determined by either Equation (18a) or (19), while Figure 11b shows the predicted shear strength determined by either Equation (18b) or (19). Figure 11a,b show similar results. Both the mean and COV shown in those figures are greater than the mean and COV shown in Figure 10. In addition, the number of data appearing above the upper dashed line in Figure 11a,b is 174 and 171, respectively, and the number of data appearing below the upper dashed line is 14 and 13 for Figure 11a,b, respectively.



(a) Either Equation (18a) or (19)



(b) Either Equation (18b) or (19)

Figure 11. Comparison between experimental and prediction results based on ACI 318-19 Equations.

In Table 7, the mean and COV values exhibited by Equation (18) can be seen. Since the fiber volume fraction in the experimental program was 1.50%, Equation (18) governed the prediction of shear strengths for all SFRC beam specimens. It can be seen that the prediction results obtained by using either Equations (18a) or (18b) are not as accurate as the results obtained by using Equation (17); however, it can be proved that Equation (18) is more conservative than Equation (17).

10. Conclusions

This study presents the results of comparison between the shear strengths of RC and SFRC beams obtained from experimental and the shear strengths obtained by using previous shear strength equations. Ten high-strength SFRC beams were prepared and tested to verify the shear strength prediction equations. The new shear strength model is proposed. In summary, the following conclusions can be drawn:

- (1) Eight equations for predicting the shear strength of SFRC beams proposed by different researchers were evaluated by using test results obtained from 236 beams. The equations considering the beam parameters affecting the shear strength are more reasonable than those not considering the parameters affecting the shear strength.
- (2) Ten high-strength SFRC beams were prepared to evaluate and verify the reviewed shear strength equations. Five of six specimens of series B1 failed in flexural followed by shear (flexural-shear failure) and one failed in shear. For the specimens of series B2, 3 specimens failed in shear prior to flexural, where the failure mode was a combination of diagonal tension and shear compression. By contrast, another beam in series B2 failed due to combination of web crushing and flexural with crushing on the top of the specimen (around the vertical load) with yielding of the longitudinal reinforcing bar.
- (3) From beams in series B1 with a longitudinal reinforcement ratio of 0.75% and 1.50% and beams in series B2, the ultimate shear strength decreased as the shear span-to-effective depth ratio increased. In addition, based on the observation of beams in series B1, improving the longitudinal reinforcement ratio increased the ultimate shear strength.
- (4) For series B1, the shear strength corresponding to the flexural strength is less than the measured shear strengths. These results almost agree with failure modes found in specimens B1, except specimen B1-2-1.5. On the other hand, the shear strength measured in series B2 tend to be similar to the shear strength corresponding to flexural strength. By referring to flexural analysis, the compression force from flexural might contribute to exhibiting crushing of the concrete on top of specimens of series B2. Accordingly, in series B2, the shear failure and compression failure due to flexure might occur simultaneously.
- (5) The basic proposed prediction equation was derived by following ACI-ASCE 326. The shear strength of SFRC beam is defined as the multiplication between shear strength of RC beam provided in ACI 318-14 and fiber effectiveness factor, in which the upper limit of shear strength of the SFRC beam is set as multiplication between $0.29 \sqrt{f'_c}$ (MPa) and fiber effectiveness factor. Combining steel fiber and RC beam parameters in one term is reasonable, since there must be an interaction between steel fibers and concrete. In the absence of steel fibers, the proposed equation is exactly the same as the detailed equation for predicting shear strength of RC beam, as provided in ACI 318-14.
- (6) Based on the results of comparison between the test results of beams provided in database and the proposed shear strength prediction equation, the results calculated by using proposed shear strength prediction equation is more conservative than those calculated by using previous shear strength equations.
- (7) The proposed shear strength prediction equation was used to predict the shear strength of beam specimens. For series B1, half of the measured shear strengths were less than the proposed

prediction shear strengths. Compared to the shear strengths of series B2, the shear strengths obtained from the proposed shear strength equation show lower results.

- (8) The proposed shear strength prediction equation can be applied for beams with a concrete compressive strength, fiber volume fraction, yield strength of longitudinal reinforcing bar, and shear span-to-effective depth ratio ranging from 20 MPa to 194 MPa, 0% to 1.5%, 420 MPa to 785 MPa, and 2.5 to 6.0, respectively.
- (9) The proposed shear strength prediction equation in this study is developed based on fiber reinforced concrete (FRC) beam with steel fiber (fiber made of steel material). Therefore, the use of proposed equation to predict FRC beam with fiber made of other materials should be further verified by conducting more experimental program on FRC beams with other types of fiber.
- (10) For alternative analysis and design of the SFRC beam, the ACI 318-19 shear strength equation is multiplied by fiber effectiveness factor. Multiplying ACI 318-19 shear strength equations with fiber effectiveness factor shows conservative results, compared to the results obtained by using proposed shear strength prediction equation.

Author Contributions: The research project described in this paper was parts of Taiwan NEW RC Project. These parts were supervised by W.-C.L.; The experimental works were conducted by W.P. and Y.-F.W.; W.P. wrote the manuscript and proposed the new equations for analysis and design of SFRC beams.

Funding: This research was sponsored by the Ministry of Science and Technology (MOST) of Taiwan under Grant Nos. 108-2221-E-002-019-MY3 and 108L892503. The opinions expressed in this paper are solely those of the authors and do not necessarily reflect the view of the sponsor.

Acknowledgments: The National Centre for Research on Earthquake Engineering (NCREE) of Taiwan is gratefully acknowledged. The authors would like to thank Shyh-Jiann Hwang from the Department of Civil Engineering at National Taiwan University. The authors would also like to appreciate Agie Vianthi who received her Master Degree in Civil Engineering in 2015 from the Department of Civil Engineering at National Taiwan University for her contribution to the experimental program. Appreciation is also extended to the Centre for Earthquake Engineering Research (CEER) at National Taiwan University.

Conflicts of Interest: The authors have no conflict of interest.

Appendix A

Table A1. Normal reinforced concrete and steel fiber reinforced concrete (SFRC) beam database.

ID	b _w (mm)	h (mm)	d (mm)	a/d	Longitudinal Reinforcement		f' _c (MPa)	Steel Fibers			v _{u,exp} (MPa)	Ref.	
					ρ (%)	f _{yt} ^(a) (MPa)		Type ^(b)	L _f /D _f	V _f (%)			f _{u,SF} ^(c) (MPa)
B18-0a	152	455	381	3.43	2.70	448	42.83	-	-	0.00	-	1.10	
B18-0b	152	455	381	3.43	2.70	448	42.83	-	-	0.00	-	1.10	
B18-1a	152	455	381	3.43	2.00	496	44.80	H	55	0.75	1100	2.90	
B18-1b	152	455	381	3.43	2.00	496	44.80	H	55	0.75	1100	2.80	
B18-2a	152	455	381	3.50	2.00	496	38.10	H	55	1.00	1100	3.00	
B18-2b	152	455	381	3.50	2.00	496	38.10	H	55	1.00	1100	3.10	
B18-2c	152	455	381	3.50	2.70	448	38.10	H	55	1.00	1100	3.50	
B18-2d	152	455	381	3.50	2.70	448	38.10	H	55	1.00	1100	2.60	
B18-3a	152	455	381	3.43	2.70	448	31.00	H	55	1.50	1100	2.60	
B18-3b	152	455	381	3.43	2.70	448	31.00	H	55	1.50	1100	3.40	
B18-3c	152	455	381	3.43	2.70	448	44.90	H	55	1.50	1100	3.30	
B18-3d	152	455	381	3.43	2.70	448	44.90	H	55	1.50	1100	3.30	
B18-5a	152	455	381	3.43	2.70	448	49.20	H	80	1.00	1100	3.00	[21,25,29]
B18-5b	152	455	381	3.43	2.70	448	49.20	H	80	1.00	1100	3.80	
B18-7a	152	455	381	3.43	2.00	496	43.30	H	80	0.75	2300	3.30	
B18-7b	152	455	381	3.43	2.00	496	43.30	H	80	0.75	2300	3.30	
B27-1a	205	685	610	3.50	2.00	455	50.80	H	55	0.75	1100	2.90	
B27-1b	205	685	610	3.50	2.00	455	50.80	H	55	0.75	1100	2.70	
B27-2a	205	685	610	3.50	2.00	455	28.70	H	80	0.75	1100	2.80	
B27-2b	205	685	610	3.50	2.00	455	28.70	H	80	0.75	1100	2.80	
B27-3b	205	685	610	3.50	1.60	448	42.30	H	55	0.75	1100	2.80	
B27-4a	205	685	610	3.50	1.60	448	29.60	H	80	0.75	1100	2.10	
B27-4b	205	685	610	3.50	1.60	448	29.60	H	80	0.75	1100	1.80	
B27-5	205	685	610	3.50	2.10	455	44.40	H	55	1.50	1100	3.50	
B27-6	205	685	610	3.50	2.10	455	42.80	H	80	1.50	1100	3.40	
B27-7	205	685	610	3.50	1.60	448	37.00	-	-	0.00	-	1.30	

Table A1. Cont.

ID	b _w (mm)	h (mm)	d (mm)	a/d	Longitudinal Reinforcement		f' _c (MPa)	Steel Fibers			v _{u,exp} (MPa)	Ref.	
					ρ (%)	f _{yl} ^(a) (MPa)		Type ^(b)	L _f /D _f	V _f (%)			f _{u,SF} ^(c) (MPa)
A00	150	250	219	2.80	1.91	610	41.20	-	-	0.00	-	1.23	[30]
A10	150	250	219	2.80	1.91	610	40.85	H	60	1.00	1115	2.93	
A20	150	250	219	2.80	1.91	610	43.20	H	60	2.00	1115	3.14	
B00	150	250	219	2.00	1.91	610	41.20	-	-	0.00	-	1.51	
B10	150	250	219	2.00	1.91	610	40.90	H	60	1.00	1115	3.50	
B20	150	250	219	2.00	1.91	610	43.20	H	60	2.00	1115	3.52	
FHB1-2	125	250	212	2.00	1.52	442	62.60	-	-	0.00	-	3.02	[17]
FHB2-2	125	250	212	2.00	1.52	442	63.80	H	62.5	0.50	1079	5.09	
FHB3-2	125	250	212	2.00	1.52	442	68.60	H	62.5	0.75	1079	5.44	
FHB1-3	125	250	212	3.00	1.52	442	62.60	-	-	0.00	-	2.53	
FHB2-3	125	250	212	3.00	1.52	442	63.80	H	62.5	0.50	1079	3.09	
FHB3-3	125	250	212	3.00	1.52	442	68.60	H	62.5	0.75	1079	3.40	
FHB1-4	125	250	212	4.00	1.52	442	62.60	-	-	0.00	-	1.98	
FHB2-4	125	250	212	4.00	1.52	442	63.80	H	62.5	0.50	1079	2.41	
FHB3-4	125	250	212	4.00	1.52	442	68.60	H	62.5	0.75	1079	2.74	
FNB2-2	125	250	212	2.00	1.52	442	30.80	H	62.5	0.50	1079	4.04	
FNB2-3	125	250	212	3.00	1.52	442	30.80	H	62.5	0.50	1079	2.55	
FNB2-4	125	250	212	4.00	1.52	442	30.80	H	62.5	0.50	1079	2.00	
A1	150	225	197	2.00	1.34	462	24.20	-	-	0.00	-	2.03	[11]
A2	150	225	197	2.80	1.34	462	24.20	-	-	0.00	-	1.52	
A3	150	225	197	3.60	1.34	462	24.20	-	-	0.00	-	1.30	
A4	150	225	197	4.40	1.34	462	24.20	-	-	0.00	-	1.14	
B1	150	225	197	2.00	1.34	462	29.10	H	60	0.50	1260	2.54	
B2	150	225	197	2.80	1.34	462	29.10	H	60	0.50	1260	1.78	
B3	150	225	197	3.60	1.34	462	29.10	H	60	0.50	1260	1.52	
B4	150	225	197	4.40	1.34	462	29.10	H	60	0.50	1260	1.29	
C1	150	225	197	2.00	1.34	462	29.90	H	60	0.75	1260	2.88	
C2	150	225	197	2.80	1.34	462	29.90	H	60	0.75	1260	2.03	
C3	150	225	197	3.60	1.34	462	29.90	H	60	0.75	1260	1.61	
C4	150	225	197	4.40	1.34	462	29.90	H	60	0.75	1260	1.39	

Table A1. Cont.

ID	b _w (mm)	h (mm)	d (mm)	a/d	Longitudinal Reinforcement		f' _c (MPa)	Steel Fibers			v _{u,exp} (MPa)	Ref.	
					ρ (%)	f _{yl} ^(a) (MPa)		Type ^(b)	L _f /D _f	V _f (%)			f _{u,SF} ^(c) (MPa)
C5	150	225	197	2.80	0.79	462	29.90	H	60	0.75	1260	1.27	[11]
C6	150	225	197	2.80	2.00	462	29.90	H	60	0.75	1260	2.20	
D1	150	225	197	2.00	1.34	462	30.00	H	60	1.00	1260	3.15	
D2	150	225	197	2.80	1.34	462	30.00	H	60	1.00	1260	2.20	
D3	150	225	197	3.60	1.34	462	30.00	H	60	1.00	1260	1.71	
D4	150	225	197	4.40	1.34	462	30.00	H	60	1.00	1260	1.49	
E1	150	225	197	2.80	0.79	462	20.60	H	60	0.75	1260	1.18	
E2	150	225	197	2.80	1.34	462	20.60	H	60	0.75	1260	1.52	
E3	150	225	197	2.80	2.00	462	20.60	H	60	0.75	1260	2.03	
F1	150	225	197	2.80	0.79	462	20.60	H	60	0.75	1260	1.58	
F2	150	225	197	2.80	1.34	462	20.60	H	60	0.75	1260	2.54	
F3	150	225	197	2.80	2.00	462	33.40	H	60	0.75	1260	2.91	
A-HSC	200	250	180	3.33	4.50	590	80.00	-	-	0.00	-	5.86	
A-NSC	200	250	195	3.08	3.10	590	45.90	-	-	0.00	-	4.38	
A-NSC _{mix}	200	250	195	3.08	3.10	590	39.40	S	75	1.00	1850	4.85	
B-HSC	200	300	235	2.77	4.30	500	85.40	-	-	0.00	-	5.96	
B-HSC _{S30/0.6}	200	300	235	2.77	4.30	500	91.40	H	50	1.00	1100	6.60	
C-HSC _{S60/0.7/0.5}	200	500	410	2.93	3.06	590	69.30	H	86	0.50	2200	3.21	
C-HSC _{S60/0.7/0.5}	200	500	410	2.93	3.06	590	69.30	H	86	0.50	2200	3.80	
C-HSC _{S60/0.7/0.75}	200	500	410	2.93	3.06	590	60.20	H	86	0.75	2200	4.13	
C-HSC _{S60/0.7/0.75}	200	500	410	2.93	3.06	590	75.70	H	86	0.75	2200	3.56	
D-HSC _{S6/0.15}	300	700	570	2.98	2.90	590	76.80	S	40	1.00	2600	2.60	
D-HSC _{S_{mix}}	300	700	570	2.98	2.90	590	72.00	S	75	1.00	1850	3.33	
D-HSC _{S60/0.7/0.75}	300	700	570	2.98	2.90	590	62.00	H	86	0.75	2200	2.98	
2/1.0/1.5	152	254	221	1.50	1.10	448	34.00	H	60	1.00	1345	3.16	[32]
2/1.0/2.5	152	254	221	2.50	1.10	448	34.00	H	60	1.00	1345	1.79	
2/1.0/3.5	152	254	221	3.50	1.10	448	34.00	H	60	1.00	1345	1.38	
2/0.5/1.5	152	254	221	1.50	1.10	448	34.00	H	60	0.50	1345	3.17	
2/0.5/2.5	152	254	221	2.50	1.10	448	34.00	H	60	0.50	1345	1.72	
2/0.5/3.5	152	254	221	3.50	1.10	448	34.00	H	60	0.50	1345	1.34	

Table A1. Cont.

ID	b _w (mm)	h (mm)	d (mm)	a/d	Longitudinal Reinforcement		f' _c (MPa)	Steel Fibers				v _{u,exp} (MPa)	Ref.
					ρ (%)	f _{yl} ^(a) (MPa)		Type ^(b)	L _f /D _f	V _f (%)	f _{u,SF} ^(c) (MPa)		
2/0/1.5	152	254	221	3.50	1.10	448	34.00	-	-	0.00	-	1.93	
2/0/3.5	152	254	221	3.50	1.10	448	34.00	-	-	0.00	-	1.17	
4/1.0/1.5	152	254	221	3.50	2.39	448	34.00	H	60	1.00	1345	4.38	
4/1.0/2.5	152	254	221	3.50	2.39	448	34.00	H	60	1.00	1345	2.45	
4/1.0/3.5	152	254	221	3.50	2.39	448	34.00	H	60	1.00	1345	2.00	[32]
4/0.5/1.5	152	254	221	3.50	2.39	448	34.00	H	60	0.50	1345	4.00	
4/0.5/2.5	152	254	221	3.50	2.39	448	34.00	H	60	0.50	1345	1.89	
4/0.5/3.5	152	254	221	3.50	2.39	448	34.00	H	60	0.50	1345	1.47	
4/0/1.5	152	254	221	3.50	2.39	448	34.00	-	-	0.00	-	2.37	
4/0/3.5	152	254	221	3.50	2.39	448	34.00	-	-	0.00	-	1.03	
B-2-1.0-L	125	250	215	2.00	0.37	500	92.00	H	75	1.00	260	1.68	
B-4-1.0-L	125	250	215	4.00	0.37	500	92.60	H	75	1.00	260	0.89	
B-6-1.0-L	125	250	215	6.00	0.37	500	93.70	H	75	1.00	260	0.56	
B-1-0.5-A	125	250	215	1.00	2.84	460	99.00	H	75	0.50	260	9.09	
B-2-0.5-A	125	250	215	2.00	2.84	460	99.10	H	75	0.50	260	4.82	
B-4-0.5-A	125	250	215	4.00	2.84	460	95.40	H	75	0.50	260	2.27	
B-6-0.5-A	125	250	215	6.00	2.84	460	95.83	H	75	0.50	260	1.95	
B-1-1.0-A	125	250	215	1.00	2.84	460	95.30	H	75	1.00	260	12.74	
B-2-1.0-A	125	250	215	2.00	2.84	460	95.30	H	75	1.00	260	6.06	[13]
B-4-1.0-A	125	250	215	4.00	2.84	460	97.53	H	75	1.00	260	3.17	
B-6-1.0-A	125	250	215	6.00	2.84	460	100.50	H	75	1.00	260	1.96	
B-1-1.5-A	125	250	215	1.00	2.84	460	96.40	H	75	1.50	260	13.95	
B-2-1.5-A	125	250	215	2.00	2.84	460	96.60	H	75	1.50	260	7.21	
B-4-1.5-A	125	250	215	4.00	2.84	460	97.10	H	75	1.50	260	3.51	
B-6-1.5-A	125	250	215	6.00	2.84	460	101.32	H	75	1.50	260	1.98	
B-2-1.0-M	125	250	215	2.00	4.58	470	94.50	H	75	1.00	260	6.73	
B-4-1.0-M	125	250	215	4.00	4.58	470	93.80	H	75	1.00	260	3.88	
B-6-1.0-M	125	250	215	6.00	4.58	470	95.00	H	75	1.00	260	2.93	
1.2/1	200	300	260	3.50	3.56	420	44.00	-	-	0.00	-	1.74	
1.2/2	200	300	260	3.50	3.56	420	46.90	H	67	0.25	1000	2.11	[33]
1.2/3	200	300	260	3.50	3.56	420	43.70	H	67	0.51	1000	2.31	
1.2/4	200	300	260	3.50	3.56	420	48.30	H	67	0.76	1000	2.98	

Table A1. Cont.

ID	b _w (mm)	h (mm)	d (mm)	a/d	Longitudinal Reinforcement		f' _c (MPa)	Steel Fibers				v _{u,exp} (MPa)	Ref.
					ρ (%)	f _{yl} ^(a) (MPa)		Type ^(b)	L _f /D _f	V _f (%)	f _{u,SF} ^(c) (MPa)		
2.2/1	200	300	260	1.50	1.81	420	40.80	-	-	0.00	-	4.03	
2.2/2	200	300	260	1.50	1.81	420	41.20	H	67	0.25	1000	5.38	
2.2/3	200	300	260	1.50	1.81	420	40.30	H	67	0.76	1000	5.76	
2.3/1	200	300	262	2.50	1.15	420	40.10	-	-	0.00	-	1.50	
2.3/2	200	300	262	2.50	1.15	420	40.00	H	67	0.25	1000	1.57	
2.3/3	200	300	262	2.50	1.15	420	38.70	H	67	0.76	1000	2.06	
2.4/1	200	300	260	2.50	1.81	420	40.10	-	-	0.00	-	2.30	
2.4/2	200	300	260	2.50	1.81	420	40.00	H	67	0.25	1000	2.07	
2.4/3	200	300	260	2.50	1.81	420	38.70	H	67	0.76	1000	2.77	
2.6/1	200	300	260	4.00	1.81	420	40.80	-	-	0.00	-	1.44	
2.6/2	200	300	260	4.00	1.81	420	41.20	H	67	0.25	1000	1.58	
2.6/3	200	300	260	4.00	1.81	420	40.30	H	67	0.76	1000	2.25	[33]
20x30-Plain-1	200	300	260	3.50	2.83	420	32.10	-	-	0.00	-	1.15	
20x30-SFRC-1	200	300	260	3.50	2.83	420	37.70	H	67	0.50	1000	2.13	
20x60-Plain-1	200	600	540	3.50	2.73	420	32.10	-	-	0.00	-	1.00	
20x60-SFRC-1	200	600	540	3.50	2.73	420	37.70	H	67	0.50	1000	1.42	
T15x100-Plain-1	200	500	460	3.40	2.80	420	32.10	-	-	0.00	-	1.65	
T15x100-SFRC-1	200	500	460	3.40	2.80	420	37.70	H	67	0.50	1000	2.65	
20x30-SFRC-2	200	300	260	3.50	2.83	420	38.80	H	67	0.50	1000	2.53	
20x60-SFRC-2	200	600	540	3.50	2.73	420	38.80	H	67	0.50	1000	2.05	
T10x50-SFRC-2	200	500	460	3.40	2.80	420	38.80	H	67	0.50	1000	1.70	
T15x50-SFRC-2	200	500	460	3.40	2.80	420	38.80	H	67	0.50	1000	1.78	
T23x50-SFRC-2	200	500	460	3.40	2.80	420	38.80	H	67	0.50	1000	2.74	
V-0-0	150	390	324	2.50	3.23	570	46.30	-	-	0.00	-	3.55	
V-1-0	150	390	324	2.50	3.23	570	58.87	H	65	1.00	1150	5.35	[34]
V-2-0	150	390	324	2.50	3.23	570	51.67	H	65	2.00	1150	5.98	
A-S28-VF0	120	220	178	3.30	5.88	520	34.52	-	-	0.00	-	2.47	
A-S28-VF1	120	220	178	3.30	5.88	520	34.52	H	65	0.40	1150	2.96	
A-S28-VF2	120	220	178	3.30	5.88	520	34.52	H	65	0.80	1150	3.67	
B-S60-VF0	120	220	178	3.30	5.88	520	61.70	-	-	0.00	-	3.79	[26]
B-S60-VF1	120	220	178	3.30	5.88	520	61.70	H	65	0.40	1150	5.73	
B-S60-VF3	120	220	178	3.30	5.88	520	61.70	H	65	1.20	1150	4.99	

Table A1. Cont.

ID	b _w (mm)	h (mm)	d (mm)	a/d	Longitudinal Reinforcement		f' _c (MPa)	Steel Fibers				v _{u,exp} (MPa)	Ref.
					ρ (%)	f _{yl} ^(a) (MPa)		Type ^(b)	L _f /D _f	V _f (%)	f _{u,SF} ^(c) (MPa)		
C-S100-VF0	120	220	178	3.30	5.88	520	95.14	-	-	0.00	-	3.04	[26]
C-S100-VF1	120	220	178	3.30	5.88	520	95.14	H	65	0.40	1150	3.93	
C-S100-VF2	120	220	178	3.30	5.88	520	95.14	H	65	0.80	1150	4.77	
C-S100-VF3	120	220	178	3.30	5.88	520	95.14	H	65	1.20	1150	5.91	
NSC1-PC	200	480	435	2.51	1.04	512	24.80	-	-	0.00	-	0.79	[35]
NSC1-FRC1	200	480	435	2.51	1.04	512	24.80	H	50	0.38	1100	1.54	
NSC2-PC	200	480	435	2.51	1.04	512	33.50	-	-	0.00	-	0.97	
NSC2-FRC1	200	480	435	2.51	1.04	512	33.50	H	50	0.38	1100	1.38	
NSC2-FRC2 *	200	480	435	2.51	1.04	512	33.50	H	64	0.50	1450	1.63	
NSC-3PC	200	480	435	2.51	1.04	512	38.60	-	-	0.00	-	0.95	
NSC3-FRC1	200	480	435	2.51	1.04	512	38.60	H	50	0.38	1100	1.62	
HSC1-PC	200	480	435	2.51	1.04	512	60.50	-	-	0.00	-	1.30	
HSC1-FRC1	200	480	435	2.51	1.04	512	61.10	H	48.00	0.64	1250	2.20	
NSC4-PC-500	200	500	455	2.51	0.99	512	25.90	-	-	0.00	0.00	1.22	
NSC4-FRC-500-1	200	500	455	2.51	0.99	512	24.40	H	50.00	0.25	1100	2.13	
NSC4-FRC-500-2	200	500	455	2.51	0.99	512	24.40	H	50.00	0.25	1100	1.69	
NSC4-PC-1000	200	1000	910	2.50	1.03	530	25.90	-	-	0.00	0.00	1.07	
NSC4-FRC-1000	200	1000	910	2.50	1.03	530	24.40	H	50.00	0.25	1100	1.42	
HSC2-PC-1000	200	1000	910	2.50	1.03	530	55.00	-	-	0.00	0.00	1.14	
HSC2-FRC-1000	200	1000	910	2.50	1.03	530	55.00	H	50.00	0.25	1100	1.86	
SFRC12W6	152	305	254	3.50	2.5	420	29.00	H	67.11	0.75	1096	3.10	[24]
SFRC12W24	610	305	254	3.50	2.5	420	29.00	H	67.11	0.75	1096	3.10	
SFRC18a	152	457	394	3.61	2.82	420	39.00	H	67.11	0.75	1096	2.70	
SFRC18b	152	457	394	3.61	2.82	420	39.00	H	67.11	0.75	1096	3.20	
SFRC24a	203	610	541	3.45	2.64	420	50.00	H	67.11	0.75	1096	2.40	
SFRC24b	203	610	541	3.45	2.64	420	50.00	H	67.11	0.75	1096	3.50	
SFRC36a	254	914	813	3.50	2.72	420	50.00	H	67.11	0.75	1096	3.30	
SFRC36b	254	914	813	3.50	2.72	420	50.00	H	67.11	0.75	1096	3.40	
SFRC48a	305	1219	1118	3.50	2.65	420	50.00	H	67.11	0.75	1096	3.10	
SFRC48b	305	1219	1118	3.50	2.65	420	50.00	H	67.11	0.75	1096	3.00	

Table A1. Cont.

ID	b _w (mm)	h (mm)	d (mm)	a/d	Longitudinal Reinforcement		f' _c (MPa)	Steel Fibers				v _{u,exp} (MPa)	Ref.
					ρ (%)	f _{yl} ^(a) (MPa)		Type ^(b)	L _f /D _f	V _f (%)	f _{u,SF} ^(c) (MPa)		
B-1-L	125	250	215	1.00	0.37	500	91.00	-	-	0.00	-	2.13	
B-2-L	125	250	215	2.00	0.37	500	90.10	-	-	0.00	-	1.14	
B-2.5-L	125	250	215	2.50	0.37	500	92.00	-	-	0.00	-	0.85	
B-3-L	125	250	215	3.00	0.37	500	90.40	-	-	0.00	-	0.74	
B-4-L	125	250	215	4.00	0.37	500	91.70	-	-	0.00	-	0.56	
B-6-L	125	250	215	6.00	0.37	500	89.50	-	-	0.00	-	0.34	
B-1-A	125	250	215	1.00	2.84	460	94.80	-	-	0.00	-	7.09	
B-2-A	125	250	215	2.00	2.84	460	94.90	-	-	0.00	-	3.35	
B-2.5-A	125	250	215	2.50	2.84	460	93.7	-	-	0.00	-	2.07	[36]
B-3-A	125	250	215	3.00	2.84	460	91.5	-	-	0.00	-	2.05	
B-4-A	125	250	215	4.00	2.84	460	92.3	-	-	0.00	-	1.90	
B-6-A	125	250	215	6.00	2.84	460	92	-	-	0.00	-	1.49	
B-1-M	125	250	215	1.00	2.84	470	93	-	-	0.00	-	10.27	
B-2-M	125	250	215	2.00	2.84	470	90.4	-	-	0.00	-	4.65	
B-2.5-M	125	250	215	2.50	2.84	470	91.2	-	-	0.00	-	2.55	
B-3-M	125	250	215	3.00	4.58	470	90.1	-	-	0.00	-	2.13	
B-4-M	125	250	215	4.00	4.58	470	90.5	-	-	0.00	-	2.05	
B-6-M	125	250	215	4.00	4.58	470	90.3	-	-	0.00	-	1.91	
NSC-I	200	300	250	3.00	3.04	750	38	-	-	0.00	-	1.5	
NSC-II	200	300	250	3.50	3.04	750	38	-	-	0.00	-	1.56	
NSC-III	200	300	250	4.00	3.04	750	36	-	-	0.00	-	1.53	
HSC-I	200	300	250	3.00	3.04	750	133	-	-	0.00	-	2.84	
HSC-II	200	300	250	3.50	3.04	750	116	-	-	0.00	-	1.86	[37]
HSC-III	200	300	250	4.00	3.04	750	114	-	-	0.00	-	1.7	
HSC-IV	200	300	250	3.00	3.04	750	165	-	-	0.00	-	4.52	
HSC-V	200	300	250	3.50	3.04	750	194	-	-	0.00	-	1.6	
HSC-VI	200	300	250	4.00	3.04	750	183	-	-	0.00	-	2.11	
A1	127	254	203.20	4.00	3.93	420	66.12	-	-	0.00	-	2.24	
A2	127	254	203.20	3.00	3.93	420	66.12	-	-	0.00	-	2.67	[38]
A3	127	254	203.20	2.70	3.93	420	66.12	-	-	0.00	-	2.67	
A7	127	254	208.03	4.00	1.77	420	66.12	-	-	0.00	-	1.77	

Table A1. Cont.

ID	b _w (mm)	h (mm)	d (mm)	a/d	Longitudinal Reinforcement		f' _c (MPa)	Steel Fibers				v _{u,exp} (MPa)	Ref.
					ρ (%)	f _{yl} ^(a) (MPa)		Type ^(b)	L _f /D _f	V _f (%)	f _{u,SF} ^(c) (MPa)		
A8	127	254	208.03	3.00	1.77	420	66.12	-	-	0.00	-	1.85	
A9	127	254	208.03	2.70	1.77	420	66.12	-	-	0.00	-	3.03	
B1	127	254	201.68	4.00	5.04	420	72.81	-	-	0.00	-	2.00	
B2	127	254	201.68	3.00	5.04	420	72.81	-	-	0.00	-	2.69	
B3	127	254	201.68	2.70	5.04	420	72.81	-	-	0.00	-	3.91	
B7	127	254	208.03	4.00	2.25	420	72.81	-	-	0.00	-	1.69	
B8	127	254	208.03	3.00	2.25	420	72.81	-	-	0.00	-	1.77	
B9	127	254	208.03	2.70	2.25	420	72.81	-	-	0.00	-	3.03	[38]
C1	127	254	184.15	4.00	6.64	420	69.92	-	-	0.00	-	2.32	
C2	127	254	184.15	3.00	6.64	420	69.92	-	-	0.00	-	3.23	
C3	127	254	184.15	2.70	6.64	420	69.92	-	-	0.00	-	2.95	
C7	127	254	206.50	4.00	3.26	420	69.92	-	-	0.00	-	1.73	
C8	127	254	206.50	3.00	3.26	420	69.92	-	-	0.00	-	1.70	
C9	127	254	206.50	2.70	3.26	420	69.92	-	-	0.00	-	1.73	
FC1	150	610	558	1.60	2.12	420	60	-	-	0.00	-	1.78	
FC2	150	610	558	1.60	2.12	420	54.10	H	60	0.75	1200	3.30	
FC3	150	610	558	1.60	2.12	420	49.90	H	60	1.50	1200	3.87	
FC4	150	610	558	1.60	2.12	420	60	-	-	0.00	-	0.59	
FC5	150	610	558	1.60	2.12	420	54.1	H	60	0.75	1200	2.83	
FC6	150	610	558	1.60	2.12	420	49.9	H	60	1.50	1200	3.32	[39]
FC7	150	610	558	1.60	2.12	420	57	-	-	0.00	-	1.46	
FC8	150	610	558	1.60	2.12	420	54.8	H	60	0.40	1200	2.44	
FC9	150	610	558	1.60	2.12	420	56.5	H	60	0.60	1200	2.77	
FC10	150	610	558	1.60	2.12	420	46.9	H	100	0.40	1200	2.95	
FC11	150	610	558	1.60	2.12	420	40.8	H	100	0.60	1200	2.83	

- (a) In the absence of yield strength of longitudinal reinforcing bar, f_{yl} is assumed as 420 MPa
- (b) Fiber type: H = hooked-end steel fiber, S = straight steel fiber
- (c) Fu = steel fiber tensile strength

References

1. Lee, H.J.; Chen, J.H. *Testing of Mechanical Splices for Grade 685 Steel Reinforcing Bars*; TTK Report; NCREC: Taipei, Taiwan, 2014; pp. 54–88.
2. Liao, W.C.; Perceka, W.; Liu, E.J. Compressive Stress-Strain Relationship of High Strength Steel Fiber Reinforced Concrete. *J. Adv. Concr. Technol.* **2015**, *13*, 379–392. [[CrossRef](#)]
3. Cusson, D.; Paultre, P. High Strength Concrete Column Confined by Rectangular Ties. *J. Struct. Eng.* **1994**, *120*, 783–804. [[CrossRef](#)]
4. Cusson, D.; Paultre, P. Stress-Strain Model for Confined High-Strength Concrete. *J. Struct. Eng.* **1995**, *121*, 468–477. [[CrossRef](#)]
5. ACI Committee 318. *Building Code Requirements for Structural Concrete (ACI 318-14) and Commentary*; American Concrete Institute: Farmington Hills, MI, USA, 2014.
6. Fanella, D.A.; Naaman, A.E. Stress-Strain Properties of Fiber Reinforced Mortar in Compression. *J. Tech. Pap.* **1985**, *82*, 475–483.
7. Hsu, L.S.; Hsu, C.T. Stress-Strain behavior of steel fiber reinforced concrete under compression. *Struct. J.* **1994**, *91*, 448–457.
8. Mansur, M.A.; Chin, M.S.; Wee, T.H. Stress-Strain Relationship of High Strength Fiber Concrete in Compression. *J. Mater. Civ. Eng.* **1999**, *11*, 21–29. [[CrossRef](#)]
9. Perceka, W.; Liao, W.C.; Wang, Y.D. High Strength Concrete Columns Under Axial Compression Load: Hybrid Confinement Efficiency of High Strength Transverse Reinforcement and Steel Fibers. *Materials* **2016**, *9*, 264. [[CrossRef](#)]
10. Sharma, A.K. Shear Strength of Steel Fiber Reinforced Concrete Beams. *J. Tech. Pap.* **1986**, *83*, 624–628.
11. Mansur, M.A.; Ong, K.C.G.; Paramasivam, P. Shear Strength of Fibrous Concrete Beams without Stirrups. *J. Struct. Eng.* **1986**, *112*, 2066–2079. [[CrossRef](#)]
12. Narayanan, R.; Darwish, I.Y.S. Use of Steel Fibers as Shear Reinforcement. *Struct. J.* **1987**, *84*, 216–227.
13. Ashour, S.A.; Hasanain, G.S.; Wafa, F.F. Shear Behavior of High Strength Fiber Reinforced Concrete Beams. *Struct. J.* **1992**, *89*, 176–184.
14. Imam, M.; Vandewalle, L.; Mortelmans, F.; Gemert, D.V. Shear Domain of Fiber Reinforced High Strength Concrete Beams. *Eng. Struct.* **1997**, *19*, 738–747. [[CrossRef](#)]
15. Parra-Montesinos, G.J. Shear Strength of Beams with Deformed Steel Fibers. *Concr. Int.* **2006**, *28*, 57–67.
16. Aoude, H.; Belghiti, M.; Cook, W.D.; Mitchell, D. Response of Steel Fiber-Reinforced Concrete Beams with and without Stirrups. *Struct. J.* **2012**, *109*, 359–367.
17. Kwak, Y.K.; Eberhard, M.O.; Kim, W.S.; Kim, J. Shear Strength of Steel Fiber Reinforced Concrete Beams without Stirrups. *Struct. J.* **2012**, *99*, 530–538.
18. Naaman, A.E.; Najm, H. Bond-Slip Mechanisms of Steel Fibers in Concrete. *Mater. J.* **1992**, *88*, 135–145.
19. Cho, S.H.; Kim, Y.I. Effects of Steel Fibers on Short Beams Loaded in Shear. *Struct. J.* **2003**, *100*, 765–774.
20. Thomas, J.; Ramaswamy, A. Mechanical Properties of Steel Fiber Reinforced Concrete. *J. Mater. Eng.* **2007**, *19*, 385–392. [[CrossRef](#)]
21. Dinh, H.H. Shear Behavior of Steel Fiber Reinforced Concrete Beams without Stirrup Reinforcement. Ph.D. Dissertation, College of Engineering—Civil and Environmental Engineering Department, University of Michigan, Ann Arbor, MI, USA, 2009.
22. Swamy, R.N.; Jones, R.; Chiam, A.T.P. Influence of Steel Fibers on The Shear Resistance of Lightweight Concrete I-Beams. *Struct. J.* **1993**, *90*, 103–114.
23. Swamy, R.N.; Bahia, H.M. Influence of Fiber Reinforcement on the Dowel Resistance to Shear. *Symp. Pap.* **1979**, 327–355.
24. Zarrinpour, M.R.; Chao, S.H. Shear Strength Enchantment Mechanisms of Steel Fiber Reinforced Concrete Slender Beams. *Struct. J.* **2017**, *114*, 729–742. [[CrossRef](#)]
25. Dinh, H.H.; Parra-Montesinos, G.J.; Wight, J.K. Shear Strength Model for Steel Fiber Reinforced Concrete Beams without Stirrup Reinforcement. *J. Struct. Eng.* **2011**, *137*, 1039–1051. [[CrossRef](#)]
26. Al Rawashdeh, O.J.Z. Shear Behavior of Steel-Fiber Reinforced Ultra-High-Strength Self-Compacted Concrete Beams. Master's Thesis, College of Engineering—Department of Civil and Environmental Engineering, United Arab Emirates University, Abu Dhabi, UAE, 2015.

27. Swamy, R.N.; Mangat, P.S.; Rao, C.V.S.K. *The Mechanic of Fiber Reinforcement of Cement Matrices*; Detroit: Fiber Reinforced Concrete—Special Publication (SP-44); American Concrete Institute: Farmington Hills, MI, USA, 1974.
28. Wu, Y.F. Evaluation of Flexural and Shear Capacity of High Strength Steel Fiber-Reinforced Concrete Beams without Stirrups. Master's Thesis, College of Engineering—Department of Civil Engineering, National Taiwan University, Taipei, Taiwan, 2014. (In Chinese).
29. Dinh, H.H.; Parra-Montesinos, G.J.; Wight, J.K. Shear Behavior of Steel Fiber-Reinforced Concrete Beams without Stirrup Reinforcement. *Struct. J.* **2010**, *107*, 597–606.
30. Cucchiara, C.; La-Mendola, L.; Papia, M. Effectiveness of Stirrups and Steel Fibers as Shear Reinforcement. *Cem. Concr. Comp.* **2004**, *26*, 777–786. [[CrossRef](#)]
31. Noghabai, K. Beams of Fibrous Concrete in Shear and Bending: Experiment and Model. *J. Struct. Eng.* **2000**, *126*, 243–251. [[CrossRef](#)]
32. Lim, T.Y.; Paramasivam, P.; Lee, S.L. Shear and Moment Capacity of Reinforced Steel-Fiber Concrete Beams. *Mag. Concr. Res.* **1987**, *39*, 148–160. [[CrossRef](#)]
33. Lin, A.L. Prediction of Shear Strength of Fiber Reinforced Concrete Beam of Intermediate Shear Span. Master's Thesis, College of Engineering—Department of Civil Engineering, National Taiwan University, Taipei, Taiwan, 2013. (In Chinese)
34. Araujo, D.d.L.; Nunes, F.G.T.; Filho, R.D.T.; de Andrade, M.A.S. Shear Strength of Steel Fiber-Reinforced Concrete Beams. *Acta Sci. Tech. Mar.* **2014**, *36*, 380–397. [[CrossRef](#)]
35. Minelli, F.; Plizzari, G.A. On the Effectiveness of Steel Fibers as Shear Reinforcement. *Struct. J.* **2013**, *110*, 379–390.
36. Wafa, F.F.; Ashour, S.A.; Hasanain, G.S. Shear Behavior of Reinforced High Strength Concrete Beams without Shear Reinforcement. *Eng. J. Qatar Univ.* **1994**, *7*, 91–113.
37. Perera, S.V.T.J.; Mutsuyoshi, H. Shear Capacity of Reinforced High-Strength Concrete Beams without Web Reinforcement. In Proceedings of the Thirteenth East Asia-Pacific Conference Structural Engineering and Construction (EASEC-13), Hokkaido University, Sapporo, Japan, 11–13 September 2013.
38. Ahmad, S.H.; Khaloo, A.R.; Poveda, A. Shear Capacity of Reinforced High-Strength Concrete Beams. *J. Tech. Pap.* **1986**, *83*, 297–305.
39. Adebar, P.; Mindess, S.; St-Pierre, D.; Olund, B. Shear Test of Fiber Concrete Beams without Stirrups. *Struct. J.* **1997**, *94*, 68–76.
40. ACI Innovation Task Group 4. *Report on Structural Design and Detailing for High-Strength Concrete in Moderate to High. Seismic Applications (ITG-4.3R-07)*; American Concrete Institute: Farmington Hills, MI, USA, 2007.
41. Naaman, A.E. Toughness, Ductility, Surface Energy, and Deflection-Hardening FRC composites. Tokyo, Japan. Proceeding: Ductile Fiber Reinforced Cementitious Composites (DFRCC). *J. Concr. Inst.* **2002**, *33*–57.
42. ACI Committee 544. *Guide to Design with Fiber-Reinforced Concrete*; American Concrete Institute: Farmington Hills, MI, USA, 2018.
43. Joint ACI-ASCE Committee 326. Shear and Diagonal Tension. *J. Proc.* **1962**, *59*, 279–333.
44. Perceka, W. Shear Behavior of High Strength Steel Fiber Reinforced Concrete Columns. Doctoral Dissertation, College of Engineering—Department of Civil Engineering, National Taiwan University, Taipei, Taiwan, 2019. (In English)
45. ACI Committee 318. *Building Code Requirements for Structural Concrete (ACI 318-19) and Commentary*; American Concrete Institute: Farmington Hills, MI, USA, 2019.

